A TRIDENT SCHOLAR PROJECT REPORT

NO. 513

**Acoustic Manipulation of Microrobots
Using Chladni Plates and Multimode Membrane Resonators**

by

Midshipman 1/C Lillian N. Usadi, USN

UNITED STATES NAVAL ACADEMY
ANNAPOLIS, MARYLAND

REPORT DOCUMENTATION PAGE

1. REPORT DATE *(DD-MM-YYYY)* 7/12/21	2. REPORT TYPE	3. DATES COVERED *(From - To)*

4. TITLE AND SUBTITLE	5a. CONTRACT NUMBER
Acoustic Manipulation of Microrobots Using Chladni Plates and Multimode Membrane Resonators	
	5b. GRANT NUMBER
	5c. PROGRAM ELEMENT NUMBER

6. AUTHOR(S)	5d. PROJECT NUMBER
Usadi, Lillian N.	
	5e. TASK NUMBER
	5f. WORK UNIT NUMBER

7. PERFORMING ORGANIZATION NAME(S) AND ADDRESS(ES)	8. PERFORMING ORGANIZATION REPORT NUMBER

9. SPONSORING / MONITORING AGENCY NAME(S) AND ADDRESS(ES)	10. SPONSOR/MONITOR'S ACRONYM(S)
U.S. Naval Academy Annapolis, MD 21402	
	11. SPONSOR/MONITOR'S REPORT NUMBER(S) Trident Scholar Report no. 513 (2021)

12. DISTRIBUTION / AVAILABILITY STATEMENT

This document has been approved for public release; its distribution is UNLIMITED.

13. SUPPLEMENTARY NOTES

14. ABSTRACT

Acoustics, the physics of vibrational waves through matter, offers a precise, accurate, and minimally invasive technique to manipulate microrobots or microparticles (stand-ins for microrobots). One example is through the use of flexural vibrations induced in resonant structures such as Chladni plates. In this research, we developed a platform for precise two-dimensional microparticle manipulation via acoustic forces arising from Chladni figures - nodal patterns - and resonating microscale membranes. The project included two distinct phases: (1) macroscale manipulation with a Chladni plate in air and (2) microscale manipulation using microscale membranes in liquid. In the first phase (macroscale in air), we reproduced previous studies in order to gain a better understanding of the underlying physics and to develop control algorithms based on statistical modeling techniques. In the second phase (microscale in liquid), we developed and tested a new setup using custom microfabricated structures. The macroscale statistical modeling techniques were integrated with microscale autonomous control systems. It is shown that control methods developed on the macroscale can be implemented and used on the microscale with good precision and accuracy.

15. SUBJECT TERMS

Chladni plates, multimode membrane resonators, acoustic actuation, microrobots, acoustics

16. SECURITY CLASSIFICATION OF:			17. LIMITATION OF ABSTRACT	18. NUMBER OF PAGES	19a. NAME OF RESPONSIBLE PERSON
a. REPORT	b. ABSTRACT	c. THIS PAGE		59	19b. TELEPHONE NUMBER *(include area code)*

U.S.N.A. --- Trident Scholar project report; no. 513 (2021)

ACOUSTIC MANIPULATION OF MICROROBOTS
USING CHLADNI PLATES AND MULTIMODE MEMBRANE RESONATORS

by

Midshipman 1/C Lillian N. Usadi
United States Naval Academy
Annapolis, Maryland

Certification of Advisers Approval

Professor Samara L. Firebaugh
Associate Provost for Academic Affairs

Associate Professor Hatem ElBidweihy
Electrical and Computer Engineering Department

LT Steven C. Yee, USN
Electrical and Computer Engineering Department

Professor Murray S. Korman
Physics Department

Acceptance for the Trident Scholar Committee

Professor Maria J. Schroeder
Associate Director of Midshipman Research

USNA-1531-2

1 Abstract

The advent of micro/nanorobotics promises to transform the physical, chemical, and biological domains by harnessing opportunities otherwise limited by size. Most notable is the biomedical field in which the ability to manipulate micro/nano particles has numerous applications in biophysics, drug delivery, tissue engineering, and microsurgery.

Acoustics, the physics of vibrational waves through matter, offers a precise, accurate, and minimally invasive technique to manipulate microrobots or microparticles (stand-ins for microrobots). One example is through the use of flexural vibrations induced in resonant structures such as Chladni plates.

In this research, we developed a platform for precise two-dimensional microparticle manipulation via acoustic forces arising from Chladni figures - nodal patterns - and resonating microscale membranes. The project included two distinct phases: (1) macroscale manipulation with a Chladni plate in air and (2) microscale manipulation using microscale membranes in liquid. In the first phase (macroscale in air), we reproduced previous studies in order to gain a better understanding of the underlying physics and to develop control algorithms based on statistical modeling techniques. In the second phase (microscale in liquid), we developed and tested a new setup using custom microfabricated structures. The macroscale statistical modeling techniques were integrated with microscale autonomous control systems. It is shown that control methods developed on the macroscale can be implemented and used on the microscale with good precision and accuracy.

Keywords: Chladni plates, multimode membrane resonators, acoustic actuation, microrobots, acoustics

2 Acknowledgements

As I type this last bit of my Trident report, I cannot help but feel overwhelming gratitude for so many who have supported me over this past year and a half journey, my first foray into scientific research. At times I felt overwhelmed and unsure of my progress. But I was guided through this treacherous journey.

First and foremost, I would like to thank my Trident advisors–LT Steven Yee, Professor Hatem ElBidweihy, Professor Samara Firebaugh, and Professor Murray Korman–for supporting me in all ways. From helping me with graduate school applications to answering anxiety-filled emails timestamped in the wee hours of the morning, my Trident advisors have been a source of inspiration, always challenging me to strive for excellence. LT Yee spent hours combing through my papers and editing my posters, helping me better articulate my vision while making me a better researcher. Professor Elbidweihy always had a solution for whatever road blocks we encountered. Professor Firebaugh never failed to provide a big-picture perspective. Professor Korman, introduced me to the world of acoustics.

There are many others who have had a profound impact on me, including Professor Wrage, LT Amador, LT Washkewicz, Professor Anderson, LCDR Lust, and LT Melville. Thank you to Rabbi Ballaban for being such a wonderful teacher and for guiding me in many aspects of life. Thank you to all my 2nd Companymates, Jewish Midshipmen Club members, and USNA Symphony Orchestra and Trident Brass musicians.

I would also like to thank my fellow Trident scholars: Elizabeth Gergal, Joe Wiedemann, Logan Williams, and Alec Engl for inspiring me to be a better scientist and person. Thank you to my best friends Sara and Melinda for your kindness and support.

Big thanks go to my sister Hannah and brother Benjamin for always rooting for me even though I can be "annoying" on occasion or so they claim. And of course, as always, my biggest thanks go to my parents for everything. Though we have not seen each other in-person since around the start my research (due to Singaporean COVID-19 travel restrictions), I know our reunion will be even sweeter when the time comes.

Contents

List of Figures

3   Introduction

Micro/nanorobotics have transformed the physical, chemical, and biological domains by utilizing their size (around 10^{-3} to 10^{-6} m) to navigate usually inaccessible spaces. Particularly in the biomedical field, the ability to manipulate micro/nano particles has numerous applications, including biophysics [12], drug delivery, tissue engineering [21], and microsurgery [15]. The most direct application of the manipulation of microrobots in two-dimensions are lab-on-a-chip systems [22]. Lab-on-a-chip systems allow the user to complete laboratory functions such as particle manipulation on the microscale (see Figure 3.1).

Figure 3.1: Lab-On-A-Chip has the ability to integrate various laboratory functions onto a small chip. Microrobots have great potential for use in this application [2].

Extending beyond biomedicine, microrobotic systems have attracted the attention of various entities, including the U.S. Navy. Specifically, the U.S. Navy has solicited proposals in order to further research in microassembly (additive manufacturing) [4]. The idea includes using a swarm of microrobots to autonomously construct and assemble new materials. Recently, Defense Advanced Research Projects Agency (DARPA) launched an initiative to stimulate research in microrobots for use in disaster relief [6].

One domain of microrobotics is tetherless microrobotic systems on the order of magnitude of 10^{-6} to 10^{-3} m. Tetherless microrobots are able to explore, image, and access parts of the remote parts of the human body. However, the difficulty of utilizing microrobots is manipulating and controling them remotely. While macroscale robots are often self-actuated, propelled through onboard power and actuation systems, microrobots are not often self-actuated in order to preserve their size. Self-actuation often requires a power source and mechanical parts that result in a robot beyond the scale of a microrobot. Thus, it is necessary to utilize remote manipulation methods to manipulate microrobots, but many of these methods are considered invasive.

Currently, optical [31], chemical [10], electrical [9], and magnetic [24] techniques have

been developed in an effort to control microrobots [16]. In the optical realm, optical tweezers provide accuracy, force, and precision; however, the large laser powers required can harm biological samples. Similarly, chemical techniques have the potential to alter the molecular structure of the object itself. Chemical techniques add complexity and require a precise understanding of the chemical structures and reactions involved. Magnetic methods severely limit the materials that can be directly actuated. Electrical techniques, such as dielectrophoresis, depend on the polarization and conductivity of the manipulated object [9]. As a result of induced current, the object may experience heating, which can damage the sample involved physiologically [16].

Acoustics - the physics of sound or vibrational waves through matter - offers a promising alternative for a precise, accurate, and non-invasive technique to manipulate microrobots or microparticles. Acoustics affects any material regardless of size, transparency, or chemical composition [23]. Additionally, acoustic techniques require a simpler experimental setup versus complex optical and chemical techniques [11]. Most importantly, the use of acoustic microparticle manipulation is potentially the least invasive actuation method, allowing the precise placement of a particle without damaging the medium itself [23].

One use of acoustics is harnessing acoustic radiation pressure, which is the force generated by a pulsating object. For example, a pulsating sphere radiates isotropic and homogeneous waves into a medium, similar to what one observes when pushing one's hand out repeatedly in water. As a result, the sphere generates a pressure field outwards and ultimately an outward force on other objects in the water [17]. Other acoustic techniques for particle manipulation include using oscillating air bubbles. When subjected to resonating frequencies, air bubbles pulsate, compressing and expanding. [18].

Another acoustic manipulation technique uses flexural vibrations - bending forces - induced in resonant structures such as Chladni plates. These resonant structures serve as both the work platform and a coupling layer between the manipulated particle and an actuator, typically a piezoelectric vibrator. Chladni plates utilize a combination of forces such as **acoustic radiation, acoustic streaming, and effective weight forces** to displace particles on their surface and can be used to manipulate those particles to a desired position. Chladni plate-based manipulation compares favorably to many acoustic techniques that require multiple acoustic transducers. Some designs have included as many as 64 acoustic transducers [8]. The placement and synchronization of these multiple actuators is non-trivial and results in additional system complexity. However, the use of vibrating membranes such as Chladni plates, which serve as the actuation mechanism and the work platform for the microrobot, requires the use of only **one actuator**. By allowing for precise manipulation with a simple hardware set, Chladni plates are a particularly promising means of effective particle manipulation.

4 Project Goals and Objectives

The intent of my project was to develop a platform for precise two dimensional microparticle manipulation in a fluid via acoustic forces arising from Chladni figures. This is ground-breaking research in not only acoustics, but also the biomedical realm. This research combines control methodologies proven at the macroscale with microscale actuators in order to develop a fully controllable microparticle manipulation system. The microparticle manipulation system initially focuses on moving a cluster of particles due to the difficulty of isolating a single particle. Follow up research would be conducted in two dimensional manipulation of a **single** particle, essentially serving as the model microrobot.

This project was organized in two phases: (1) Macroscale Manipulation with Chladni Plate in Air and (2) Microscale Manipulation with Microscale Membranes in Liquid (see Figure 4.1).
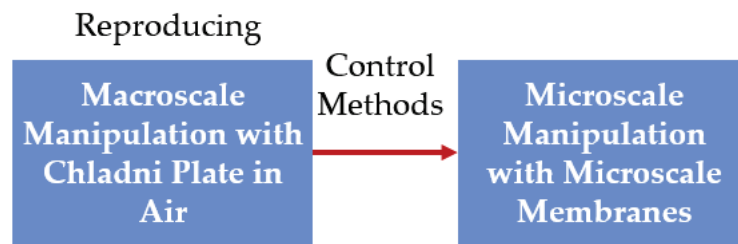
Figure 4.1: Project Phase Planning

The macroscale manipulation in air was largely a reproduction of previous studies [19] [30], which was a necessary step to later implement similar methodologies on the microscale. The reproduction validated the control methods proposed in the literature for macroscale manipulation. This project ultimately used the same control methods to manipulate particles on the microscale. The novelty of this proposed project lies in Phase 2 involving the microscale particle manipulation with microscale membranes in liquid. This effort involved the design and testing of custom micro-fabricated structures and coupling of macroscale statistical modeling with microscale autonomous control systems. Developing a microscale manipulation capability at USNA also provided a useful test bed for follow-on projects related to autonomous particle manipulation.

The project objectives were as follows:

1. To develop the experimental capability at USNA to perform two dimensional macroparticle manipulation through the use of a macroscale Chladni plate.

2. To use statistical analysis based on empirical observation of particle movement on the Chladni plate to create displacement field maps and couple it with robust closed-loop feedback control techniques to achieve macroscale autonomous control systems.

3. To develop the experimental capability at USNA to perform two dimensional microparticle manipulation in liquid through the use of custom micro-fabricated structures.

4. To use statistical analysis based on empirical observation of the movement of microparticles on the custom micro-fabricated structures to fully explain and model the underlying physics. To the author's knowledge, this field of study is incomplete and the existing literature cannot fully explain the nature of the movement of the microparticles in such a setup.

5. To couple microscale theory and models developed with control techniques to achieve microscale autonomous control systems.

Ultimately, we were able to manipulate particles on the macroscale utilizing image object identification and displacement map generation algorithms. However, on the microscale microfluidic phenomena complicated previous methods. We were able to develop accurate displacement maps on the microscale in fluid. For the future, we will be working towards being able to manipulate microrobots/microparticles on the microscale.

5 Background

5.1 Acoustics

Acoustics is often referred to as the study of sound. However, more broadly speaking, acoustics is the study of vibrational waves, extending beyond audible sound ($\sim$20 kHz) into ultrasound (above 20kHz) and beyond.

One important concept within acoustics is the idea of resonance. Resonance is the phenomena in which an oscillating system increases in amplitude when a force of the same natural periodicity of the system is applied [17]. One example of resonance is pushing a child on a swing. The length of the swing from the pivot point directly affects the period of swinging motion. If one pushes the child at time intervals that do not align with the natural periodicity of the swing, the child's swinging motion will decrease and not be maximized. However, if one pushes the child at time intervals that do align with the natural periodicity of the swing, the child's swinging motion will increase and be maximized.

5.2 Chladni Plates

Chladni plates owe their name to German physicist and musician Ernst Chladni. In his famous experiment in 1787, Chladni discovered that when he drew his violin bow over the side of a flat plate affixed to a thin post with particles of sand resting on top (see Figure 5.1), the particles moved to form symmetrical, visual patterns later named **Chladni Figures** [25]. A violin or any string instrument utilizes this phenomena. By drawing a bow over the plate or string, friction forces cause the plate and string to vibrate at a resonant frequency, ultimately creating standing wave patterns. In Chladni's experiment, sand patterns arose from different modes of resonance. Upon excitation, the sand would move away from the positions of maximum displacement (antinodes) and conform to locations of minimum displacement (nodes) [29].
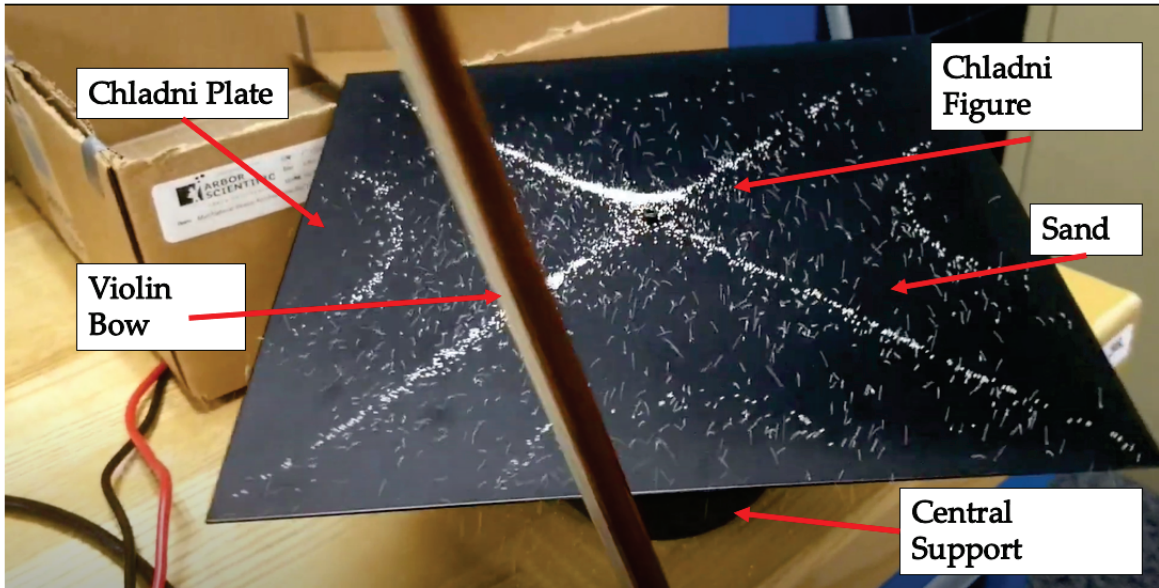
Figure 5.1: Reproduction of the original experiment Ernst Chladni conducted in which a violin bow was drawn over the side of a Chladni Plate. Sand on the plate displaced into patterns resulting from vibrations induced by the bow on the plate.
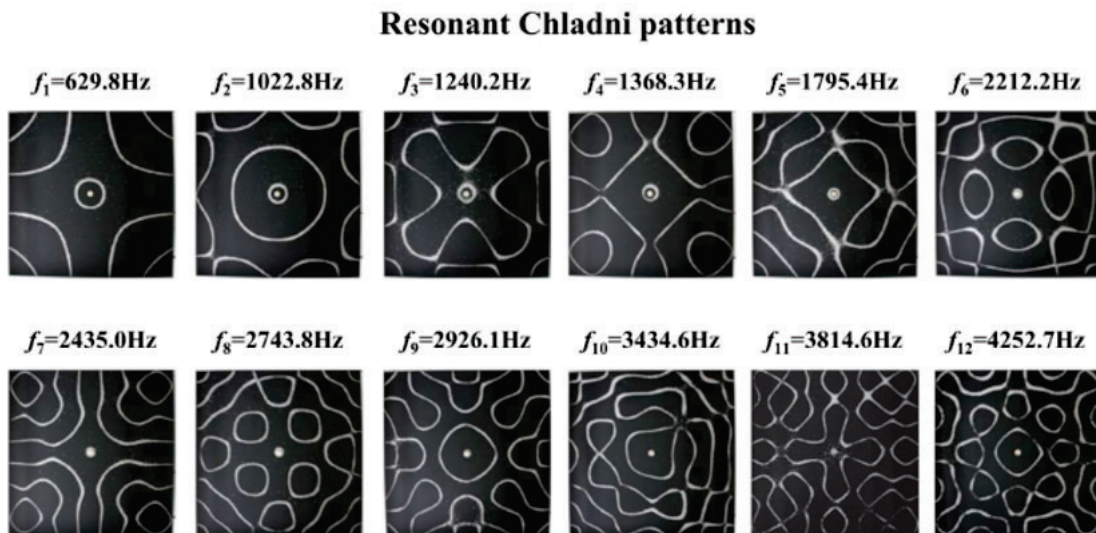
Figure 5.2: Different resonant modes of Chladni Plates visible in the patterns developed by particles on the plate surface when the plate is excited by notes of different frequencies. Reprinted with permission from Tuan *et al.* Copyright 2015, Acoustic Society of America [26].

Macroscale manipulation of particles on a Chladni plate utilizes dynamic acoustic pressure fields that arise from varying the driving frequency. One is be able to manipulate an

object's motion on a two-dimensional plane by driving the Chladni plate with a sequence of frequencies or notes. The use of Chladni plates has advantages over other acoustofluidic techniques due to the wide spectrum of frequencies that can be applied, including both resonant and non-resonant frequencies. Additionally, complex manipulation may be achieved with fewer actuators than other approaches. The mechanism relies on the forces arising from the patterns of standing waves that are drawn on the entirety of the plate, requiring only a single actuator [19].

Several studies have already used the resonant modes of Chladni plates to manipulate particles. The following sections (5.3 - 5.5) will give a brief overview of **past research** done with (1) Macroscale Manipulation with Chladni Plate in Air, (2) Macroscale Manipulation with Chladni Plate in Liquid, and (3) Microscale Manipulation with Microscale Membranes in Liquid.

5.3   Macroscale Manipulation with a Chladni Plate in Air

Initially, particle motion resulting from Chladni figures was thought to be unpredictable and difficult to model due to the complexity of the wave models and the interactions between particles and the Chladni plate. However, by using empirical and statistical means, particle motion resulting from Chladni figures in air has been predicted, modelled, and controlled by researchers in Aalto University in Finland [30]. In [30], Chladni plates were used to manipulate not only one particle with a desired trajectory to an intended position, but also multiple particles with individual, arbitrary trajectories at once.

5.4   Macroscale Manipulation with a Chladni Plate in Liquid

Building upon the research in particle manipulation on Chladni plates in air, there has been research in particle manipulation on Chladni plates in liquid. While the manipulated particles were still considered macroscale in size (100 micrometers or larger), the medium was a liquid. In one 2019 study, scientists from Aalto University manipulated heavy particles (750 μm) on a Chladni Plate submerged in water [19]. Interestingly, the liquid affected the behavior of the particles on the plate relative to the behaviors observed when manipulating particles with Chladni Plates in air. The particles moved to the **antinodes**, locations of maximum motion, rather than the nodes, positions of least motion, of the Chladni plate. The dominating force that determined the trajectory of the particle was the **particle's effective weight** [19]. Thus, instead of forming classic Chladni figures, the particles on the plate were found to form inverse Chladni figures.

5.5   Microscale Manipulation with Microscale Membranes in Liquid

The microscale manipulation of particles (10 to 100 μm) has been described previously in other studies [16, 15, 29, 20]. However, the control theory used on the macroscale (larger

than 100 μm) has not been implemented on the microscale. Similar to the Chladni plate's transition to liquid, the transition to the microscale regime adds complexity. For one, the acoustic pressure becomes negligible, and two main forces dominate: (1) acoustic streaming force and (2) mechanical vibration induced acceleration [15]. The novelty of this project was attempting to combine the control theory replicated and validated on the macroscale with microscale actuation techniques.

6 Theory

6.1 Macroscale Manipulation with Chladni Plate in Air

Harnessing Chladni Plates for macroscale manipulation requires an understanding of the flexural bending vibrations of the plate.

6.1.1 Chladni Plates

Chladni's experiment demonstrates the classical understanding of resonant frequencies operating on a macro-Chladni plate in air. While Chladni used a violin bow to stimulate standing waves in his experimental system, we instead used a piezoelectric actuator attached to the center of the plate as shown in Figure 6.1.
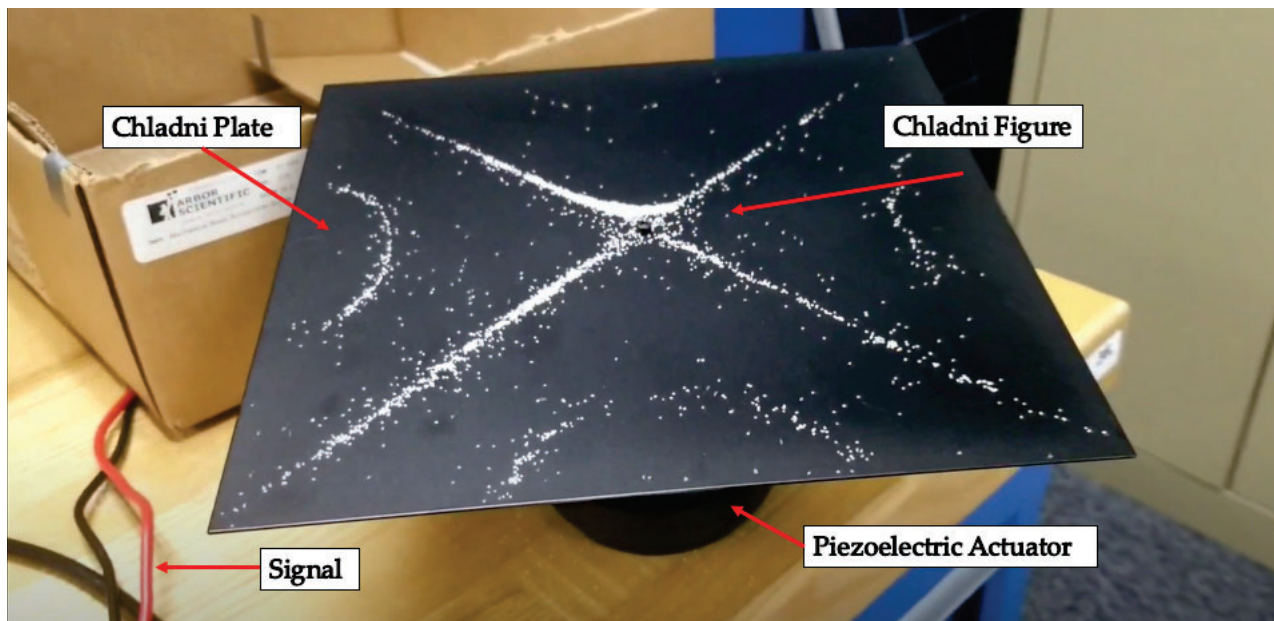
Figure 6.1: Chladni Plate with a piezoelectric actuator attached to the bottom of a Chladni Plate, instead of a central support used in Ernst's Chladni experiment

A piezoelectric actuator converts electrical signals into mechanical motion either with unidirectional displacement or with an oscillating motion. By applying a DC voltage, it is

possible to expand or compress a piezoelectric actuator. By applying a sinusoidal signal, it is possible to oscillate a piezoelectric actuator rapidly and over a range of frequencies. A plate attached on top of a vibrating piezoelectric actuator experiences flexural vibrations. At the plate's resonant frequencies, determined by properties of the plate (e.g. size, shape, stiffness) and its boundary conditions (e.g. clamped or non-clamped edges, position of actuator, etc.), the plate will experience a standing wave (Figure 6.2.a).
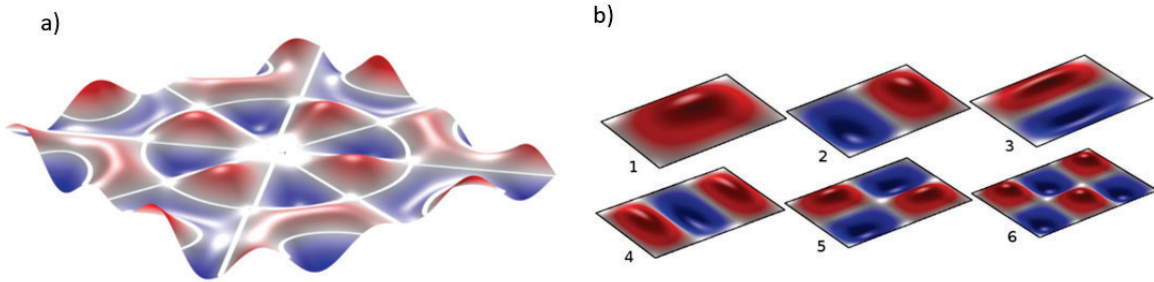
Figure 6.2: a) Chladni Plate vibrating at an eigenmode as result of excitation at an eigenfrequency b.) Different simulated eigenmodes of a Chladni plate at increasing eigenfrequencies. Plate #6 is driven at a higher frequency than plate #5, and plate #5 is driven at a higher frequency than plate #4, and so forth [14].

Chladni figures are the visual display of the **eigenmodes** - natural movement or motion of a system when driven at the corresponding eigenfrequencies - resonant frequencies - of the Chladni Plate. **Eigenfrequencies**, also known as natural frequencies, are the set of discrete frequencies at which a system has natural resonances [1]. These frequencies consist of the fundamental frequency (i.e. lowest frequency) and its harmonic multiples thereof. However, not all eigenfrequencies are multiples of one another, and a system can have multiple, separate eigenfrequencies. **Eigenmodes** are the shapes that arise from a system oscillating at a given eigenfrequency. As certain discrete eigenfrequencies are played, the Chladni plate will vibrate at the corresponding eigenmodes as shown in Figure 6.2.a. As the frequency increases, the Chladni figures become more complex. Figure 6.2.b) displays the eigenmodes of a Chladni plate at increasingly higher eigenfrequencies such that Chladni plate #6 oscillates at a higher eigenfrequency than Chladni plate #5 that oscillates at a higher eigenfrequency than Chladni plate #4 and so forth.

Mathematically, the flexural vibrations of the thin plate can be approximated using the two dimensional inhomogeneous Helmholtz Equation – the time independent form of the wave equation:

$$(\Delta^2 + k^{-2})\Psi(\mathbf{r};\mathbf{r}',\tilde{k}) = F(\mathbf{r}') \tag{1}$$

where

$$\tilde{k} = k + i\gamma \tag{2}$$

k is the wave number, γ is the damping coefficient, $\Psi(\mathbf{r}; \mathbf{r}', \tilde{k})$ is the response function of the plate, and $F(r')$ is the driving source [26].

The Helmholtz Equation can be used to calculate the corresponding eigenmodes and eigenfrequencies. $f(k)$ is the resonant frequency, C is some constant, and k is the wave number:

$$f(k) = C * k^2 \tag{3}$$

C can be calculated with the following formula

$$C = \frac{1}{2\pi} \sqrt{\frac{Ed^2}{12\rho(1 - v^2)}} \tag{4}$$

where E is Young's modulus, d is the thickness, ρ is mass density, and v is the Poisson ratio.

However, as demonstrated in [26], the resonances calculated using the above equations *do not* correspond with the experimental observations of the eigenfrequencies. This phenomenon arises from the coupling of the Chladni plate with a piezoelectric actuator. Many variables and outside influences can affect the eigenmodes of the Chladni plates. Thus, in practice the plate is subject to experimental conditions that make the resonant frequencies difficult to predict with analytical equations.

6.1.2 Modeling using COMSOL

The complexity of the multiple-order differential equations compounds the difficulty of modeling Chladni plates. However, computer simulation programs like COMSOL®Multiphysics, a finite element modeling software, make analysis relatively simple as long as the proper governing physics equations are selected and the boundary conditions and material properties specified. In past research, it is possible to create models of Chladni figures and even further on models of particle dipslacement[30]. However, because this project's purpose was to ultimately explore particle movement in uncertain experimental conditions (e.g. on the microscale in fluid), the use of COMSOL was not entirely helpful. Instead, we decided to focus on a more empirical approach to producing displacement maps (described in section 6.1.4).

One goal of this project was to construct a motion model that allows for control of particle movement on top of a vibrating Chladni plate. **Simply explained, how can we use the eigenmodes of Chladni plates to move particles?** The answer is not simple. Connecting the oscillations of a Chladni plate to the movement of particles on top of them, even in simulation, is difficult. In fact, the system becomes more complex if the medium is liquid and if the scale is shrunk to the microscale. Forces that are difficult to specify even in a computer program (e.g. acoustofluidic forces, friction, surface tension) begin to dominate. Because of the complexity and uncertainty regarding experimental details, this

project focused on empirical methods to arrive at motion models for particles on Chladni plates and membrane resonators, bypassing oversimplified analytical approaches and input-data reliant computer-based modeling.

6.1.3   Acoustofluidic Force: Acoustic Streaming

Sand is typically thought to be comprised of relatively small particles, and the particles are in fact on the order of a fraction of a millimeter. However, these dimensions are actually quite large relative to the relevant physics of a Chladni plate. In Ernst Chladni's 1787 experiment, while most sand particles moved towards the nodes, he observed that the fine shavings of his violin bow (**smaller** particles than sand) moved to the antinodes. Later that century, Michael Faraday observed the same phenomena with lycodium powder [28] and showed this strange behavior to be a result of the air current induced by the vibrating plate. This phenomena, known as "acoustic streaming", leads to complexity in manipulating the particles. Acoustic streaming will be discussed in section 6.3.1.

6.1.4   Displacement Maps - Modeling using Statistical Analysis

In order to bypass the complexity of surface, fluid, and other outside forces, scientists in studies such as [30] and [19] have used empirical means to model the movement of particles on vibrating plates. Our work also used empirical methods because ultimately, our goal was to use Chladni plates is in application. Even if the theory is not entirely understood, the controlled movement of particles can still be achieved. Through empirical research, it was also possible to observe and clarify our understanding of the theoretical phenomena and its relation to the physical one.

Suppose, a person placed one bead on top of a Chladni plate and vibrated the plate at various resonant frequencies or "notes." By taking a picture of the surface of the plate **before** the note and a picture **after** the note, it is possible to calculate a displacement vector based on the initial and final positions of a given particle. This displacement vector represents the particle's motion as a result of the note played. An arbitrary example would be a particle displacing to the right 1 mm when an F4 (349.228 Hz) note was played.

Now, suppose, a person placed many beads on top of a Chladni plate and vibrated the plate at various resonant frequencies. If the displacement vector calculations are done for particles at every point on the plate, at a very large number of frequencies, it is possible to develop a set of vector field maps displaying a displacement vector at **every** single point on the plate for all tested frequencies.

From here, how do you utilize the displacement maps to manipulate one particle to a desired position? The displacement between the current position and the intended position can be broken up into a set of waypoints. At each time step, the computer algorithm calculates many different linear combinations of displacement vectors that all end at the desired position. The weights of the note are added together from the previous accumulated weight. The note that has the most weight, meaning the note that is

most effective in moving the particle to the desired waypoint, is played. At each time step, this process is repeated until the particle reaches the desired position.

For example, Figure 6.3 is an illustration of the process just described. The blue particle follows the displacement field map of a frequency of 2.5 kHz. When the frequency changes to 3.4 kHz, the blue particles follows the vectors of the other displacement field map. Ultimately, the particles moves at first downwards and then later to the right.
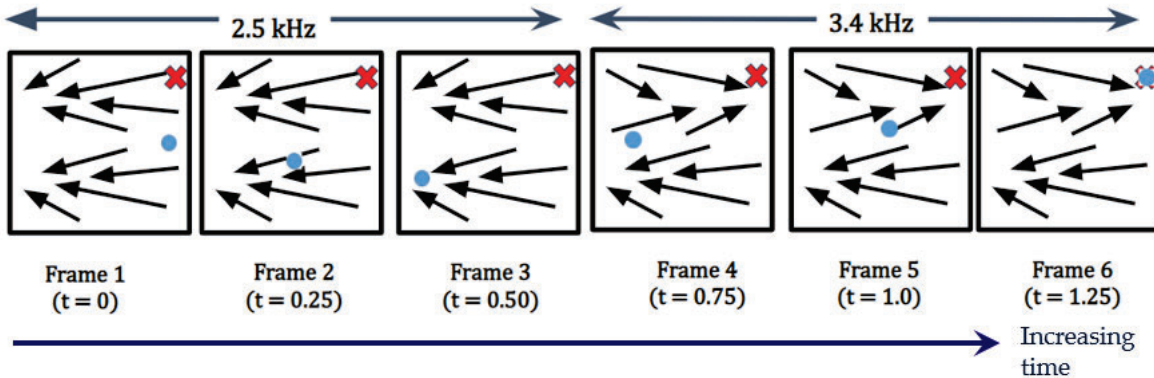
Figure 6.3: Notional schematic that shows the movement of the blue bead over time by using the displacement maps of two different frequencies.

The success of the work in [19] and [26] demonstrates that statistical modeling is a useful method to model the motion of particles on Chladni plates in an air medium. Statistical modeling bypasses the complicated physics and hidden forces that alter the movement of particles on Chladni plates. By taking pictures of beads and constructing displacement field maps, it is possible to command the motion of a particle at any point on the Chladni plate 6.4.b. One can harness the displacement field maps to move a particle to the desired position simply by selecting the notes that best correspond to the desired motion sequence.

6.2 Macroscale Manipulation with a Chladni Plate in Liquid

While the next step of the project was the microscale manipulation of particles in water (as shown in Figure 4.1), it is useful to discuss the physical phenomena present in the macroscale manipulation of particles in liquid. The introduction of liquid introduces new forces not apparent in the macroscale manipulation in air.

Macroscale manipulation of particles with a Chladni Plate submerged fully in a tank of water with a piezoelectric actuator attached to the center was previously explored[28]. The piezoelectric actuator was driven electronically via signals sent by a user or automated program via a computer. Figure 6.5 is a diagram of the experimental setup of a macroscale Chladni plate in liquid [28]).

While the flexural vibrations of the plate are similar to those observed in air, the behavior of the microparticles is not [27]. This is a result of the changed medium (liquid instead of air), resulting in the domination of different forces.
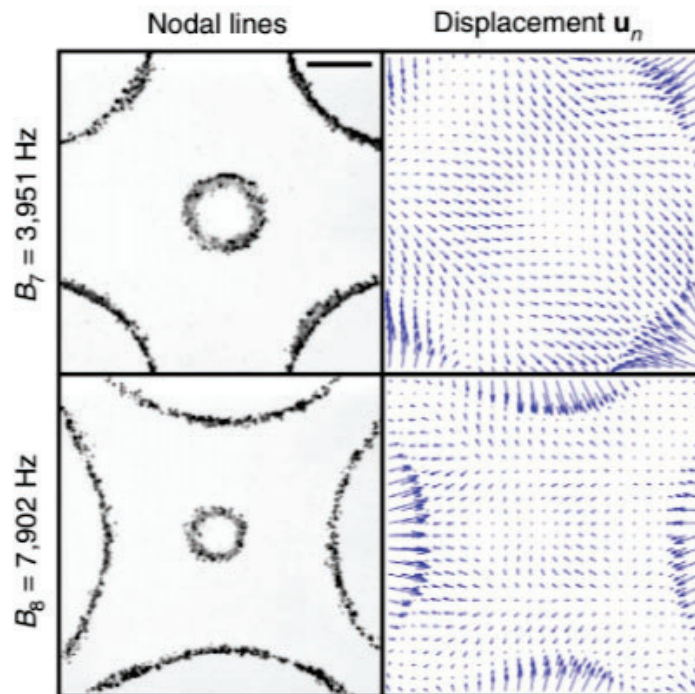
Figure 6.4: Visual representations of the nodal lines and displacement maps resulting from driving the Chladni plate with two different frequencies. The displacement maps show the direction of movement of a particle at every single point on the Chladni plate as a result of plate oscillation at the indicated frequency. [28].
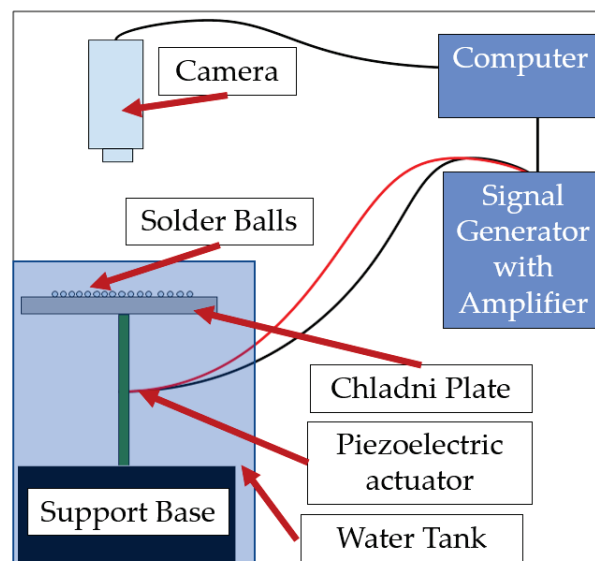
Figure 6.5: Experimental setup of a Chladni Plate in liquid.

In this experiment, macroscale particles refers to particles with diameters that are sub-mm, but larger than a micrometer (10^{-6} m). Because the vibrating plate is submerged in liquid, two forces dominate the movement of the particles: (1) the acoustic radiation force and (2) the effective weight. Intriguingly, the average of these two forces can point towards the antinodes, not the nodes [19]. The particles on the Chladni plates in liquid can move towards the antinodes, not the nodes, forming an inverted shape relative to the experiments in air. As a result of this behavior, the new patterns formed are called inverse Chladni figures. Figure 6.6 shows sand on a Chladni plate with a classic Chladni figure on the left and an inverse Chladni figure on the right.
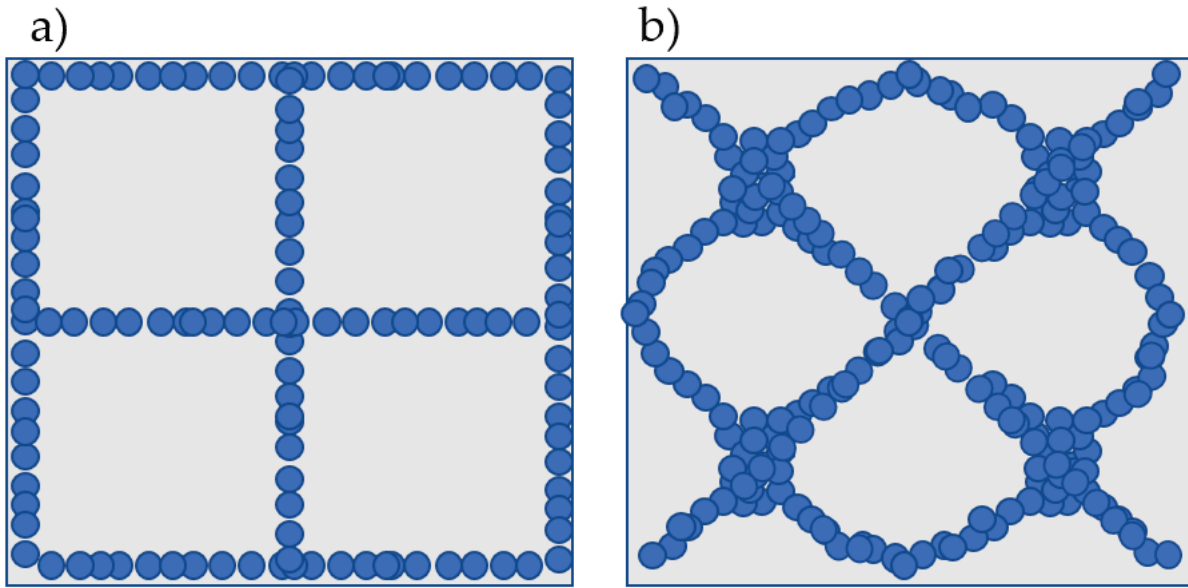
Figure 6.6: (a) Notional schematic of particles forming a classic Chladni figure (b) Notional schematic of particles forming an inverse Chladni figure [28]

6.2.1 Inverse Chladni Patterns - Acoustic Radiation Force

Acoustic radiation and acoustic streaming are strong forces that arise as a result of sound waves. However, in the macroscale manipulation of particles in liquid, the acoustic streaming force is negligible, leaving acoustic radiation as the dominant force.

Acoustic radiation is the force generated by the vibrating motion of the plate. This vibration creates a standing wave field which in turn creates an acoustic pressure wave field [19]. Through methods explained in [20] and calculated in [19], the acoustic radiation force F_r points towards the antinodal region. Thus, the particles on the submerged plate move towards the antinodes as a result of acoustic radiation.

6.2.2 Inverse Chladni Patterns - Effective Weight

Vibrational acceleration refers to the rate of change of the plate velocity. A large vibrational acceleration means that the plate oscillates quickly (higher frequency). Tuning the vibrational acceleration of the plate affects the effective weight of the particle [28]. Effective weight is the force the Chladni plate feels perpendicular to it as a result of the mass of the particle and vibrational acceleration (either greater than or less than g). Effective weight of a particle is one of the dominating forces that determines whether classical Chladni figures or inverse Chladni figures are formed. By changing the effective weight, scientists were able to control whether classical Chladni figures or inverse Chladni figures were formed. If the vibrational acceleration is larger than g and the amplitude of the oscillating plate is large, the particle will lose contact with the plate and begin to bounce. The particle will continue bouncing until it reaches a location of no movement, or a node, thus forming a classic Chladni figure (see Figure 6.6.a).

Intuitively, this explanation makes sense. If the plate bends in a downward motion faster than g, the particle will lose contact with the plate. As the plate begins to rise, the particle will still continue to fall (see Figure 6.7). At a certain point, the upward rising plate will reach the downward falling particle (see Figure 6.7.2). The transferred impulse will cause the particle to switch directions and increase its kinetic energy (see Figure 6.7.3) [28]. This motion of "bouncing" will eventually lead to the particles settling on the regions of no motion: the nodes.
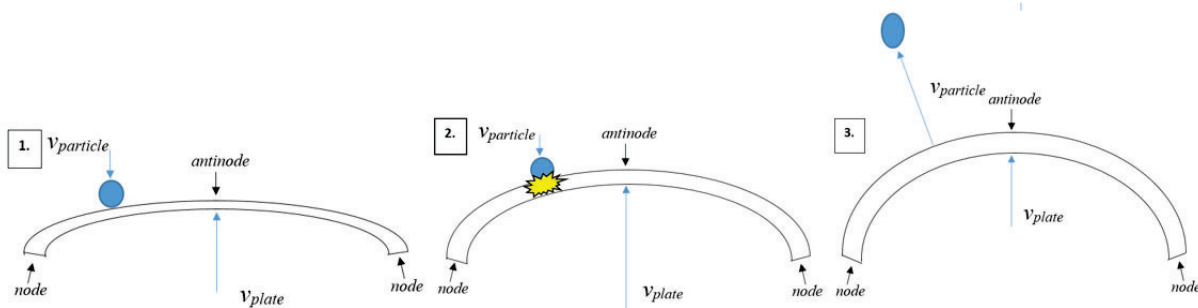
Figure 6.7: (1)As the plate begins to rise, the particle will still continue to fall. (2) Upward rising plate reaches the downward falling particle. The resulting collision leads to a transferred impulse. (3) Upward rising plate reaches the downward falling particle. The resulting collision leads to a transferred impulse.

Conversely, if the vibrational acceleration is smaller than g and the amplitude of the oscillating plate is small, the particle will be in contact with the plate at all times. This phenomenon is demonstrated in Figure 6.8.b. Instead, the particle will move to the **antinode**. For example, if the plate bends in a downward motion slower than g, the particle will remain in contact with the plate [28] and one observes a the bead rolling around the antinode. Over one vibration cycle, the average horizontal force points towards the antinode.

Mathematically, the particle effective weight **W** can modeled with the following force

equation:

$$W(x, y, t) = -m[g + \ddot{z}(x, y, t)] - F_{dz} \tag{5}$$

where (x,y) is the position of the particle, (t) is the time, m is the mass, g is the gravitational acceleration, F_{dz} is the vertical drag force that opposes the particle's motion, and z is the vertical displacement of the plate at position (x,y) [19].

The time-averaged force $\langle W_{||} \rangle$, the parallel component of $\mathbf{W}$, can be calculated with the following integral:

$$\langle W_{||} \rangle (x, y, t) = \frac{\omega}{2\pi} \int_0^{\frac{\omega}{2\pi}} W(x, y, t) \frac{dz(x, y, t)}{dx} dt \tag{6}$$

where ω is the angular frequency of the oscillation. Ultimately, $\langle W_{||} \rangle$ is the force pulling the particle towards the antinode. Through calculation as in Equation (5), it is shown that the force vector points towards the antinodal regions.
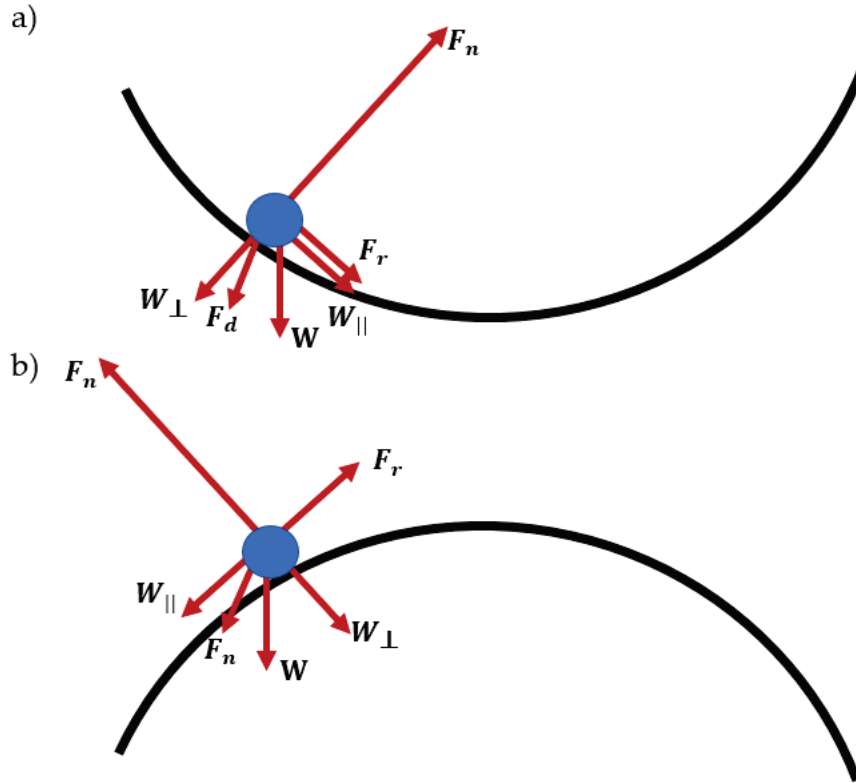
Figure 6.8: Depiction of vibrating plate where the vibrational acceleration is less than g. The average horizontal force $\langle W_{||} \rangle$ and $\mathbf{F}_r$ point towards the antinodes. $|\langle W_{||} \rangle|$ in (a) is greater than $|\langle W_{||} \rangle|$ in (b). [19]

6.2.3 Use of Nonresonant Frequencies

Although the equations above have utilized resonant frequencies, it is possible to use non-resonant frequencies to manipulate particles. The only caveat is that the plate must be vibrated with a **significantly large amplitude** [19]. Interestingly, in [19] and [29], the particles on a Chladni plate in liquid begin to move in a vortex-like motion when subjected to non-resonant frequencies. This motion was compared to a "Farandole dance."

The reason for this motion is not well understood. One explanation in [19] suggests that particles subjected to non-resonating frequencies tend to aggregate to the nearest resonating modes - closest to the non-resonating frequency. Thus, the particles move in a vortex-like pattern to the nearest resonating mode. For example in [19], the non-resonant frequency 10,675 Hz was applied with the nearest resonant frequencies at 9,575 Hz and 11,175 Hz. At resonant frequencies, the particles formed stable inverse Chladni figures. However, at non-resonant frequencies, the particles moved in the direction of the two adjacent modes. The particles moved as a result of the combination of the two different inverse Chladni figures of the adjacent modes.

6.2.4 Manipulation of Particles

As previously discussed 6.1.4, it is useful to use statistical analysis to model the movement of particles on a Chladni plate. This method is far simpler and superior than determining the particle's movement using differential equations while taking into account outside forces (e.g. friction, surface tension). Therefore, statistical analysis will again be used to model the displacement maps. The plate will be covered as uniformly as possible with heavy beads. The beads must be heavy (750 μm) in order to mitigate the buoyant force. Multiple frequencies will be played, and the movement of every bead will be recorded at every single frequency. Taking pictures before and after acoustic actuation using a given frequency, it will be possible to calculate a displacement vector for each location on the plate, generating a displacement map for the whole plate for that frequency. Thus, one is able to know the direction of motion of a single bead at any position on the plate in response to a given note. In an automated implementation, a computer algorithm could calculate many different linear combinations of displacement vectors to displace the particle to a desired position. By looping through the displacement maps, the bead will reach its desired position using the most efficient linear combination of displacement vectors.

Although the methodology for the macroscale manipulation of particles in air and liquid is the same, we expect to obtain different displacement maps for the two services. This difference should arise from the vastly different forces affecting the particle motion, including, but not limited to mechanical induced vibrational acceleration and acoustic streaming.

6.3 Microscale Manipulation Using Multimode Membrane Resonators

The second phase of the project was the **microscale manipulation in liquid using multimode membrane resonators**. Instead of using a thick (50x50x0.500 mm) Chladni plate, we used microscale silicon membranes (11.15x11.15x0.010 mm thickness) to manipulate microparticles approximately $50\mu m$ in diameter. A microscale silicon membrane was used because on the microscale, drag current and friction forces become dominant. Although microscale membranes differ from macroscale Chladni plates in terms of boundary conditions and size scales, they are comparable in that they both serve as the work platform for the manipulated particles and are a coupling mechanism between the primary source of acoustic vibration and the particles via standing wave patterns developed on the plate or membrane. At the microscale, the movement of the particles becomes difficult to predict. Unlike on the macroscale, two main forces dominate the microparticle movement: **(1) the acoustic streaming forces** and **(2) effective weight** [15]. The particle will move towards the antinode if it is dominated by streaming flow. In contrast, the particle will move towards the node if the particle is dominated by mechanical vibration induced acceleration. Sections from 6.3.1 - 6.3.2 will discuss these two phenomena.

6.3.1 Acoustic Streaming - Towards Antinodes

Acoustic streaming is the constant flow of fluid as a result of a powerful sound wave. For example, suppose a person swam next to a powerful, underwater speaker. As the speaker projects sound waves, the swimmer would feel a constant force pushing them as a result of the sound waves initially hitting the water particles, ultimately hitting the swimmer's body. Acoustic streaming is often negligible on the macroscale. However, because the microparticles ($50\mu m$) are much smaller compared to the previously described beads ($750\mu m$) or sand (1mm), the acoustic streaming force became significant.

Figure 6.9 is a visual display of the acoustic streaming force on a microparticle on a multimode membrane. Figure 6.9 is a side profile of the particle sitting on top of the membrane (color coded to indicate nodes and antinodes). Between the node and antinode (either side), the two fluid flows (upper and lower) indicated by arrows above the membrane represent the streaming flow of the fluid. In past studies, empirical observations indicate that microparticles were slightly "floating" above the membrane, ultimately subjecting the microbeads to streaming flows that result in motion towards the antinodes of the membrane [16]. However, if the particle distance from the membrane was further increased due to buoyancy or increased acceleration of the membrane, the particle would move toward the nodes due to the opposite directions of the upper and lower vortices in streaming flows depicted in Figure 6.9.
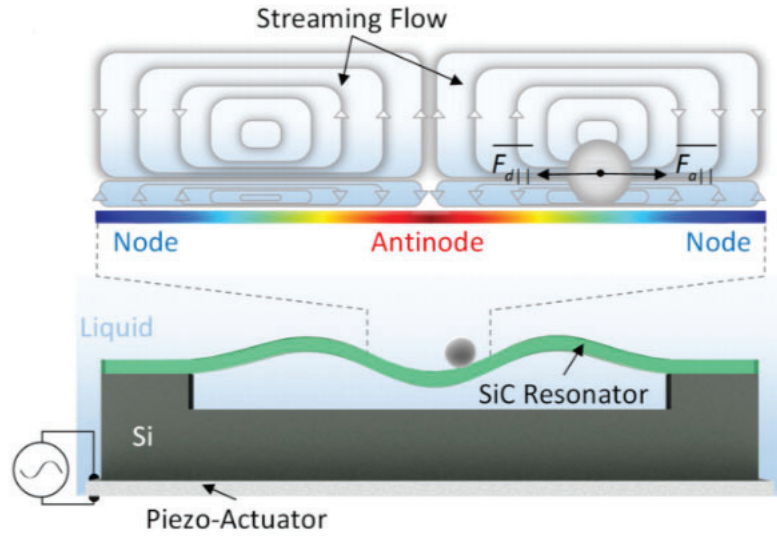
Figure 6.9: Schematic of microparticles showing forces resulting from mechanical vibration induced acceleration ($F_a||$), which point towards nodes, and forces resulting from streaming flows ($F_d||$), which point towards antinodes. Reprinted from Jia *et al.*, with the permission of AIP Publishing [16].

6.3.2 Effective Weight - Towards Nodes

Mechanical induced vibrational acceleration is the change of speed at which the membrane oscillates and **effective weight force** arises from this phenomena. As explained before, **Mechanical induced vibrational acceleration** determines the effective weight of the particle [28]. The effective weight of the particle plays a significant role in the formation of inverse or classical Chladni figures.

Currently, the leading theory concerning particle motion in liquid is that if the mechanical vibration induced acceleration dominates, the particle moves towards the nodes. However, if the streaming flow force dominates, the particle moves towards the antinodes. This explanation seems to contradict the theory concerning macroscale manipulation in liquid discussed in 6.2.2 and [16]. Before this study, the formation of standard Chladni figures on the microscale had not been proven. It seems that there are current disagreements and conflicting theories about the formation of inverse and classic Chladni figures.

6.3.3 Doubly-Clamped Beams and Square Trampoline Resonators

In past studies exploring the movement of microparticles in fluid [15][29] [16], variable membrane thickness and shape were found to play a large role in the formation of inverse and standard Chladni figures on the resonating membrane.

In a study at Case Western University, scientists observed both classic and inverse Chladni patterns formed on the sub-100μm scales [16]. Silica microparticles (1-8μm) were placed on top of two differently shaped surfaces: (1) doubly-clamped beams ($100 \times 10 \times 0.4\mu$m^3)

and (2) square trampoline resonators ($50{\times}50{\times}0.2\mu\text{m}^3$) (see Figure 6.10). The doubly-clamped beams consisted of two silicon carbide structures in parallel suspended over a silicon substrate. The doubly-clamped beams were a one dimensional configuration, meaning the nodes and antinodes of the eigenmodes conformed to linear patterns. In a straight line, a node was followed by an antinode followed by a node. With the 1D doubly-clamped beam, the beads were dominated by streaming flow ($\text{F}_d||$) and conformed to the antinodes, resulting in inverse Chladni figures.

The square trampoline consisted of resonators with square planar dimensions. However, on the square resonator, the beads were dominated by mechanical vibration induced acceleration ($\text{F}_a||$)and conformed to the nodes, resulting in standard Chladni figures (see Figure 6.10) [16]. This study demonstrates the complexity of vibration of multimode membranes in fluid. As discovered, the formation of Chladni and inverse Chladni plates depends on the shape and characteristics of the membrane, driving parameters (e.g. amplitude, frequency, etc.), and coupling phenomena (with piezoelectric actuator).
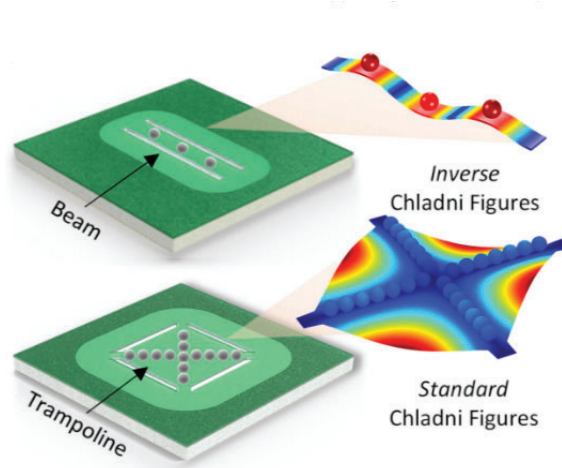
Figure 6.10: Doubly-clamped beams forming inverse Chladni Figures. Trampoline resonators forming standard Chladni Figures. Reprinted from Jia *et al.*, with the permission of AIP Publishing [16].

6.4 Autonomous Control using Statistical Modeling

The control theory is the same process as described for the experiments with Chladni plates on the macroscale (see section 6.1.4). The control theory relies heavily on image processing algorithms to detect a particle based on color, shape, and intensity. Images of the resonators are taken before and after actuation. Then, the previously obtained set of displacement field maps associated with a set of frequencies is analyzed to identify the one that best directs the particle along the desired velocity vector. By playing the note and looping through the displacement maps to find the next waypoint position, the desired position can be achieved.

As described in Section 6.1.4, displacement maps will be used to select frequencies to

manipulate the particles to desired positions. Because of the challenges of setting up an isolated particle at the microscale, it is highly likely that we will initially be manipulating swarms of particles, rather than a single one. The current position and intended position will be broken into waypoints. By looping through the displacement maps and calculating multiple paths, the note that will be most effective in moving the particles to the waypoint will be played. It will ultimately be necessary to use closed-loop feedback in order to assure the desired position is achieved within a certain error tolerance.

7   Design

7.1   Macroscale Manipulation - Chladni Plate in Air

The macroscale manipulation of microparticles (larger than 100 μm) in air has been previously demonstrated. In this work, we reproduce a previous study conducted at Aalto University to gain an understanding of the fundamentals of macroscale Chladni figures as well as test and validate statistical modeling and control techniques [30]. Although not a novel contribution, this reproduction of previous work was a useful step towards developing an integrated system for autonomous control and manipulation of microparticles in liquid. While the macroscale manipulation experiment design was largely a replication, significant design choices were required in the image acquisition and processing aspects of the project.

7.1.1   Physical Experiment Setup and Operating Frequencies

The macroscale experimental setup in this work closely mirrored that of [30], including use of the same Chladni plate dimensions and material, particle type (solder beads), piezoelectric actuator, and amplifier [30]. Sinusoidal input voltages with frequencies of 1245 Hz, 1976 Hz, 3951 Hz, 7902 Hz, 11175 Hz, and 19912 Hz were applied to the piezoelectric actuator and chosen based on their identification as the resonant frequencies of a 50mm silicon Chladni plate in [30]. Details of the experimental set up are given in Section 8.1.

7.1.2   Image Acquisition

In order to generate displacement maps, the movement of solder beads in response to notes of the aforementioned frequencies were recorded as images using a microscope camera (Dino-Lite Edge AF4115ZTW 1.3MP Digital USB Microscope 2x 50x FLC). The microscope camera was mounted directly above the Chladni plate and connected via USB to a computer. The microscope camera was instructed to record - at the fastest frame rate possible - a specified number of frames per note played. On average, solder beads required experiment time durations of 7.17 seconds over 200 frames (0.0717 seconds per frame) in order for the beads to conform to the respective Chladni figures. The amplitude of the actuation was tuned manually by adjusting the gain of a benchtop amplifier. For trials useful in the generation of displacement maps, the piezoelectric actuator required sufficient input voltage amplitude

to allow particles to conform to their respective Chladni figures, but not too much input voltage such that the piezoelectric actuator was overdriven and forced the beads off the Chladni plate. Recorded sets of frames for each note were stored in memory for later image post-processing.

7.1.3 Image Processing and Object Identification

Calibration & Cropping To facilitate the generation of displacement maps, each recorded image was processed in a consistent and automated manner using MATLAB. A projective image transformation and cropping was applied to each image in order to generate an 'overhead' view of only the Chladni plate surface while correcting for any slight misalignment of the camera and Chladni plate. The projective transform settings and image crop settings are the same for each experiment's image set and can be maintained between experiments if the plate and camera positions are not disturbed.

Image Segmentation The image was then converted from color to gray scale using MATLAB function *rgb2gray*. Then, MATLAB function *imtophat*, a morphological filter was used to correct for uneven lighting of the lab space. A 'sphere' structuring element with a diameter of 7 pixels was used in *imtophat* to morphologically filter the given image. Subsequently, pixels with intensity values less than 150 were removed. Groups of similarly colored pixels with a cluster radius less than 20 pixels were removed. Then, this image was converted into black and white (binary). The white regions were taken to correspond to detected particles or masses of particles. The black regions were taken to correspond to the background representing the absence of particles.

Object Identification The white regions corresponding to detected particles have properties that were easily computed using the built-in MATLAB function *regionprops*. A black "+" was marked on the centroid of the identified color cluster (presumably a bead) as shown in Figure 9.2. The position of each identified bead was stored in an internal MATLAB structure which was later used in the creation of displacement maps (see Section 7.1.4).

7.1.4 Displacement Maps

The binary image sets with detected objects were then used to create displacement maps as described in Section 6.1.4. It was possible to compare the position of a single particle between successive images by estimating that a detected object in one frame corresponded to the object in the next frame that had the nearest centroid image location to that of the object in the original frame. We used this estimate under the assumption that the frame rate of the recording was fast enough that particle displacement was minimal between successive frames and that excess information was not lost in the filtering process. However, at times, the frame rate was so much faster than the particle movement, the particle displacement was too small to be noticeable both to the observer and the computer algorithm. The seemingly lack of movement was accounted for in the displacement map computational code explained later on in this section.

In order to obtain regular, tabulated data, the image area corresponding to the Chladni plate was split into a 30x30 grid. All displacement vectors within a given gridsquare for any frame in the experiment image set were averaged (i.e. binned). The average, binned results are useful as effective 'look-up' tables for subsequent control experiments.

Displacement Map Algorithm Improvements

In order to work around excessively high frame rates, we explored using different frame intervals between image-pairs (e.g. Frame 1 and 2, Frame 1 and 6, etc.) when computing displacement vectors. It was possible to compute a more noticeable change in position. Additionally, processing fewer frames decreased computation time. For example, as opposed to comparing immediate subsequent frames (e.g. Frames 1 and 2) exclusively, we also computed displacement vectors based on larger frame spacing (e.g. Frames 1 and 6). Larger image-pair frame spacings reduced post-image processing time and improved displacement vector field fidelity by tracking the larger trend in displacement. This approach was supported in part by the fact that the beads conformed to patterns, rather than continuously flowing onto and off of the Chladni plate.

7.2 Microscale Manipulation - Multimode Membrane Resonators in Water

Following the macroscale experiments, we transitioned to the microscale manipulation of microrobots.

7.2.1 Multi-user MEMS Process

We designed custom microscale resonators within a multi-user MEMS process in order to realize these microscale devices with specific dimensions and within a reasonable time frame for the project. Custom dimensions were required since no known commercial alternatives existed. While it was possible to construct the microscale membrane in-house at USNA, training and fine tuning microfabrication processes would take several months, delaying researching, and reducing the potential for scientific contribution of this project. Therefore, we decided to utilize a multi-user fabrication process for microelectromechanical systems, or MEMS. MEMS can be fabricated through various means, most of which are similar to the technologies used to manufacture integrated circuits [3]. These methods make use of bulk manufacturing methods where many devices are formed in parallel through the use of common steps, which drives economies of scale and reduces the fabrication cost per device. These are essentially layer-by-layer processes where material is removed or added to each layer in areas that are defined by a photolithographic mask. Multiple users share a process flow by combining their mask sets which will determine where layers of material are added or removed.

7.2.2 PiezoMUMPS⒭ Layers

This project utilized PiezoMUMPs⒭ a silicon-on-insulator micromachining process available from MEMSCAP⒭ [5]. The substrate material was an n-type Silicon-On-Insulator wafer with an upper silicon layer thickness of $10\mu m$ separated from the bulk substrate ($100\mu m$) by a silicon oxide layer ($1\mu m$). The substrate was then selectively etched from the backside of the wafer to create suspended structures as defined by a photolithographic mask. The process also included two metal layers that also could be used for electrical contacts as well as an aluminum nitride piezoelectric layer - none of which were used in our designs. There were a total of six different layers used in the construction of the chip: Pad oxide ("PADOXIDE"), Piezoelectric material ("PZFILM"), Pad Metal ("PADMETAL"), Silicon ("SOI"), Oxide, and the Substrate ("TRENCH"). Because the chip needed to contain only various shaped membranes, the pad oxide, piezoelectric, and oxide layer were not used. A conceptual figure of the structure built is shown in Figure 7.1.b. We designed square and rectangular membrane resonators and experimented with both dimensions and boundary conditions for these resonators as detailed in Section 7.2.4. In total, 19 identical 11.25mm×11.25mm chips - each subdivided into four physically separable quadrants featuring 10-20 resonators - were fabricated.

7.2.3 PiezoMUMPS⒭ Construction Constraints
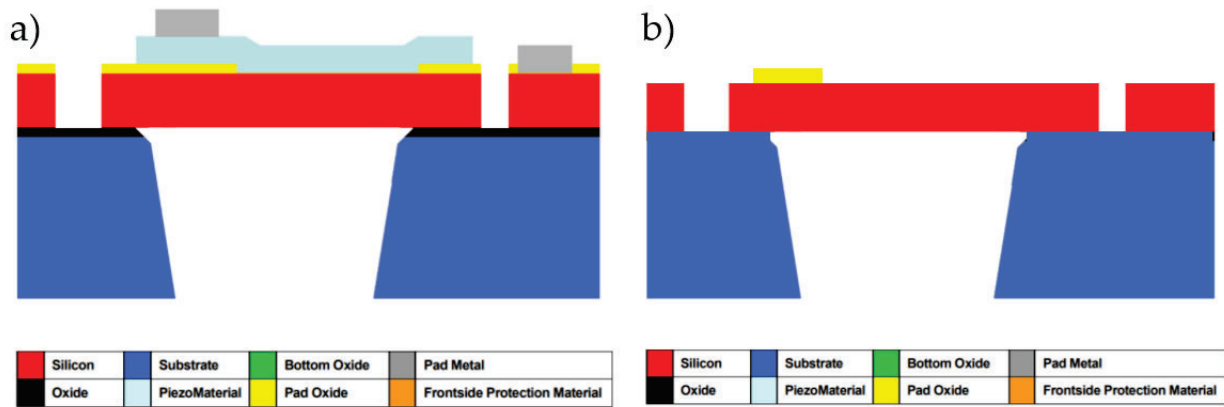
Figure 7.1: a) Notional schematic showing a stock image of a PiezoMUMPs⒭ chip b) Notion schematic showing the acutal chip design [7]

The design and layout of the chip was constrained by the process design rules. In the etching away process, an excess of removal of material would create an unstable membrane. Thus in accordance with the MEMSCAP⒭ design rules, only 33% of the material could be etched away (i.e. "TRENCH" mask layer). The design of the MEMSCAP⒭ chip required a balance of utilizing the chip area while creating a stable, robust device.
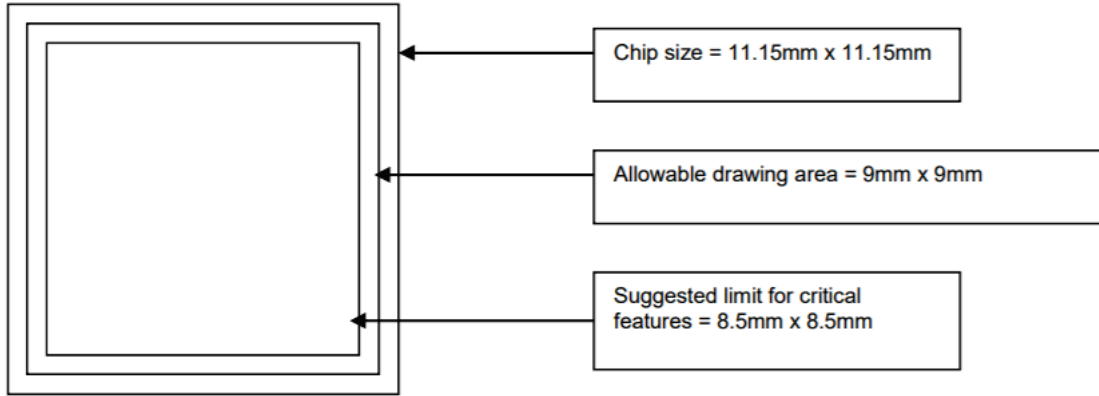
Figure 7.2: Schematic showing the usable chip area [7]

In addition, different layers (e.g. "TRENCH," "PADOXIDE," "SOI," etc.) had constraints on the minimum distance needed between features made of a specific material/layer. For example, two features constructed of Pad Metal and Silicon layer ("PADMETAL" to "SOI" layer) respectively needed to have 5μm space center to center [7]. Figure 7.1 shows a sample chip and various layers at the end of the chip construction.

The chip also contained four connected quadrants that were able to be separated by-hand. In order to allow for a seamless break without damaging the chip membranes themselves, the boundaries between each quadrant were designed with a "train-track" pattern in a "+" configuration in accordance with the design constraints laid out in [7]. This is called subdicing. Figure 7.3 shows a photograph of the set of completed microchips. The actual design of our chip will be explored in Section 7.2.4.

7.2.4 Chip Quadrants' Design and Layout

Our design included four quadrants, each of which was used to explore various shapes of resonators. Different shapes resonated at different frequencies. Within the same shape, different boundary conditions affected the resonant frequencies. We tested primarily square (2-D) and long rectangular (1-D) membrane resonators as seen in [15] and shown in Figures 7.5 to 7.7. We tested these resonators with two different boundary conditions: clamped and unclamped. In the clamped case, the 10μm silicon membrane boundary was entirely bounded on all four of its sides. In the unclamped case, the 10μm silicon membrane boundary was almost entirely unbounded on all four of its sides except for at the four corners. The 2-D bounded membrane resonator was referred to as the "Drumhead." The 2-D unbounded membrane resonator was referred to as the "Trampoline." We repeated the same concept at different geometry scales to allow us to investigate variations of the resonant frequency with different membrane planar dimensions.

A Trident logo, representative of the USNA electrical and computer engineering department as well as the Trident program, was added on the silicon membrane with the PADMETAL layer.
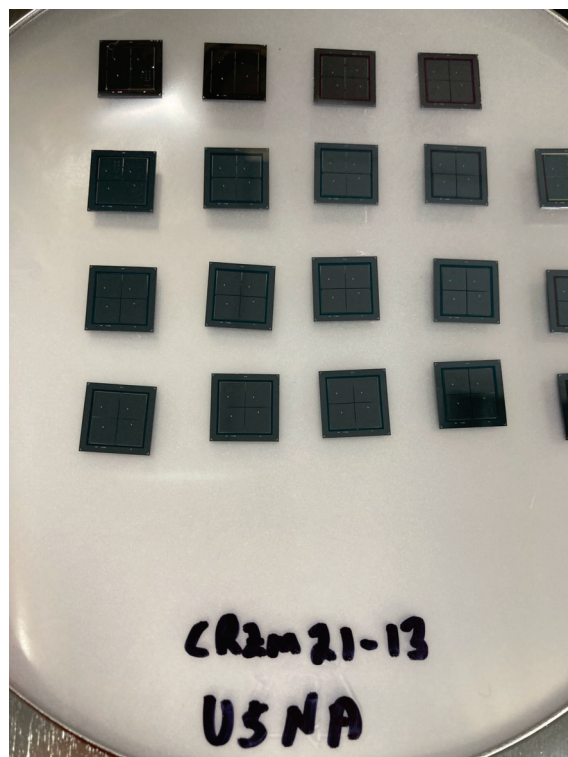
Figure 7.3: Manufactured microchips in the delivered packaging before being used.
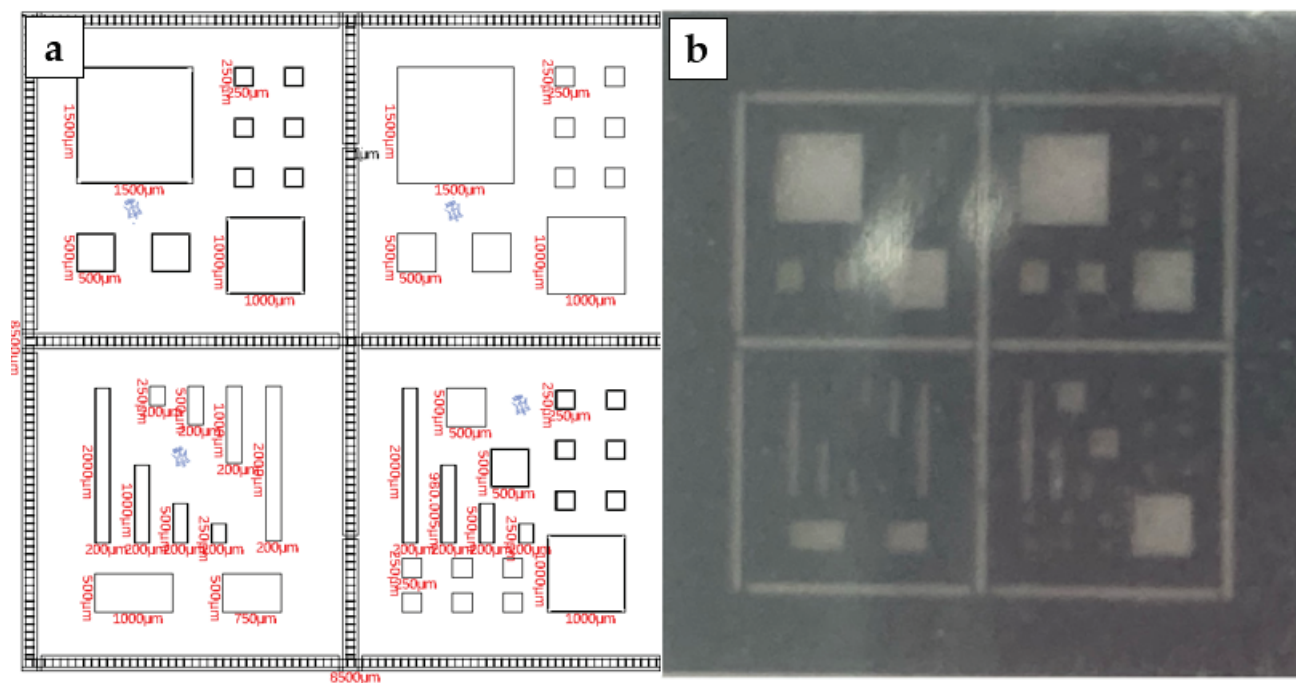
Figure 7.4: a) Microscale membrane design for a complete chip comprised of four quadrants. b) Photograph of microscale membrane, viewed from the bottom to clearly see the membrane outlines.

Quadrant 1: 2-D Drumhead (Clamped) The first quadrant (shown in Figure 7.5) explores various sizes of clamped 2-D drumhead resonators, that is all boundaries of the membranes are fastened to the chip. Figure 7.5.b is uniformly dark, and the membranes are difficult to see because there are no slits in the membrane. The photograph only shows a dark membrane and the Trident outline because light was not able to be reflected back by the material underlying the slits.
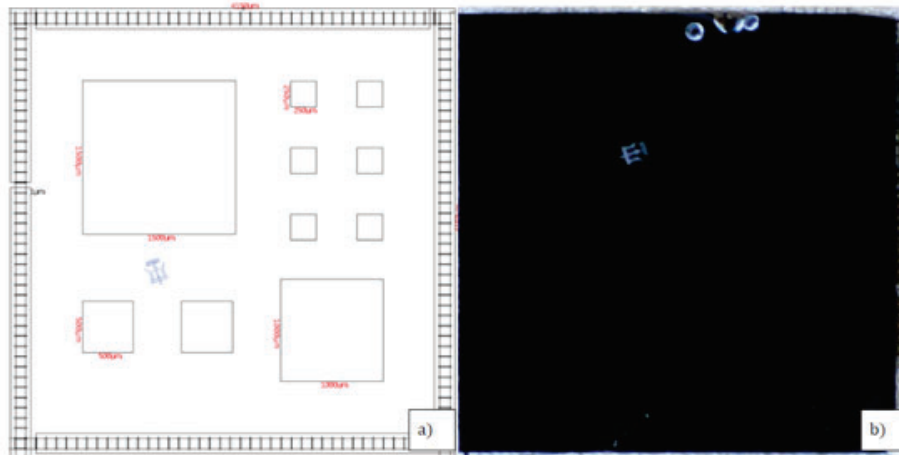
Figure 7.5: 2-D Drumhead (Clamped) a) Layout Editor Design b) Front-view photograph

Quadrant 2: 2-D Trampoline (Unclamped) The second quadrant (shown in Figure 7.6) explores the various sizes of an unclamped 2-D trampoline. The edges indicate slits etched near the borders of the suspended membranes to create unclamped edges. This boundary condition was expected to result in resonant modes with lower frequencies and larger motion amplitudes than clamped (drumhead) membrane resonators of the same planar dimensions. Figure 7.6.b shows the faint outline of each membrane. The actual effects of these slits will be discussed in the experiment itself.
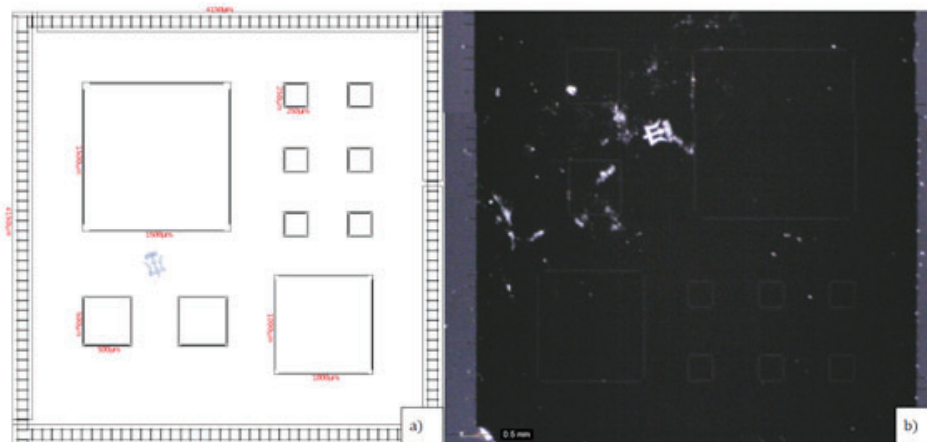
Figure 7.6: 2-D Trampoline (Unclamped) a) Layout Editor Design b) Front-view photograph

Quadrant 3: 1-D Beam (Clamped and Unclamped) The third quadrant shown in Figure 7.7, explores clamped and unclamped 1-D membrane resonators of various sizes. The shape of the membranes are rectangles of different sizes.
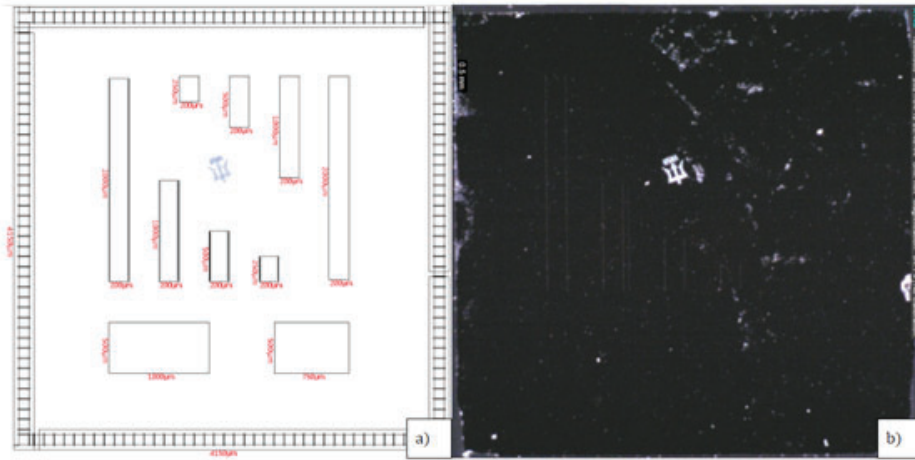
Figure 7.7: 1-D Beam (Clamped and Unclamped) a) Layout Editor Design b) Front-view photograph

Quadrant 4: Mixed (Clamped and Unclamped) The fourth quadrant as shown in Figure 7.8 incorporates designs from Figures 7.5 to 7.7. The purpose of this arrangement was to observe whether the response on the given membranes was significantly affected by its arrangement relative to other membranes on the same quadrant.
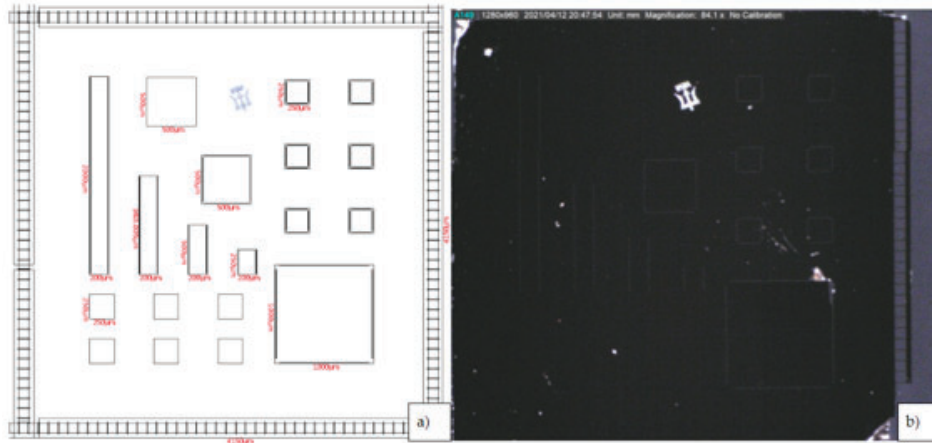
Figure 7.8: **2-D Drumhead (Clamped), 2-D Trampoline (Unclamped) and 1-D Beam (Unclamped and Clamped)** a) Layout Editor Design b) Front-view photograph

7.2.5   Frequency Analysis and Computation

We investigated order of magnitude estimates of resonant frequencies for various resonant membrane structures in different media using a combination of methods. First, we used ana-

lytical methods and finite element analysis simulation (COMSOL®) to predict the resonant frequencies of the various structures in an air medium. We specifically explored the 2-D drumhead (clamped) and trampoline (unclamped) shapes of different sizes using Equation 4).

We then used a finite element analysis simulation (COMSOL™) to model both the 2-D Drumhead (Clamped) and Trampoline (Unclamped), and we obtained good agreement between analytical methods (Equation 4) and finite element simulations (COMSOL™). We relied on finite element simulations to determine the in-air resonances of more complex geometries such as the unclamped trampoline resonators. We simulated different scenarios including a "lowest mode" and "X mode." The "lowest" mode referred to the lowest frequency that was able to induce resonance in the membrane. The "X" mode referred to the frequency that induced the typical "X" shaped Chladni figure on the membrane. After deriving the in-air resonant frequencies, We estimated the resonant frequencies in water by using a virtual mass incremental (NAVMI) factor that accounted for the weight of water[13] [15]. We estimated NAVMI factors based on literature for relatively similar structures and fluids [15] to predict how the resonant frequencies may change when the media is changed to water. By considering a water factor ranging from 0.17 - 1.87 based on the multimode membranes' design, it was possible to estimate resonant frequencies based off of membrane length, size, width, and boundary conditions[15].

The resonant frequencies that were predicted to induce resonance in the PiezoMUMPS® in air and water using analytical equations, COMSOL®, and NAVMI factors are shown in Table 1 to Table 8. The resonant frequencies of these resonators were predicted to be on the order of magnitude of 10^5 Hz and 10^6 Hz, which were comparable to those reported in [15]. In [15], Jia *et al.* tested the multimode resonances of a silicon rectangular membrane ($3000x120\mu m^2$) using frequencies 100 kHz - 1 MHz (also on the order of magnitude of 10^5 Hz and 10^6 Hz).

One thing to note, a thin membrane was expected to be driven at much lower frequencies (approximately 100 kHz to 1MHz), than with a thicker membrane (approximately 10-100 MHz) [15]. 10 to 100 MHz frequencies are utilized by surface acoustic wave (SAW) devices, whereas 100 kHz to 1MHz frequencies harness the boundary induced streaming forces (acoustic streaming).

An image of the COMSOL®ouput was generated for a 2-D Drumhead (Clamped) and Trampoline (Unclamped) at 2.21 MHz and 58.154 kHz respectfully (see Figure 7.10) with the dimensions of 1.5mm×1.5mm×10μm. The COMSOL® modeling gave us confidence that the range frequencies that were intended on being used were indeed resonant.
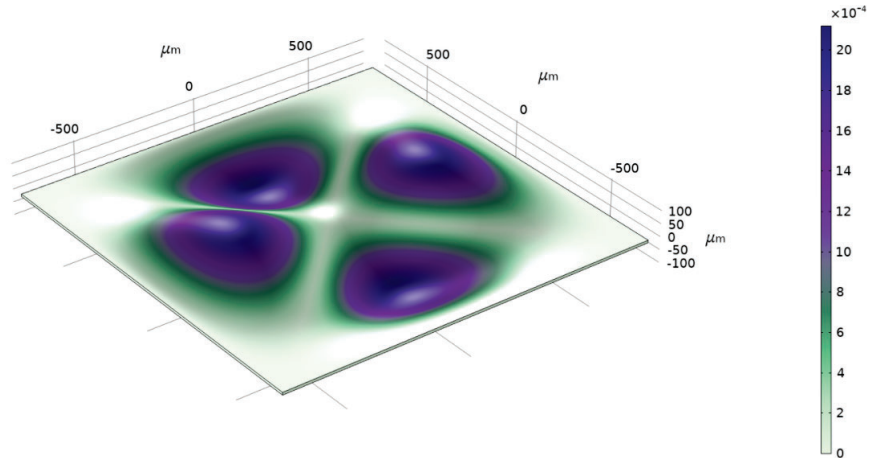
Figure 7.9: Eigenmode of a 1.5mm×1.5mm×10μm Drumhead (Clamped) in Air at 2.21 MHz modeled using COMSOL®
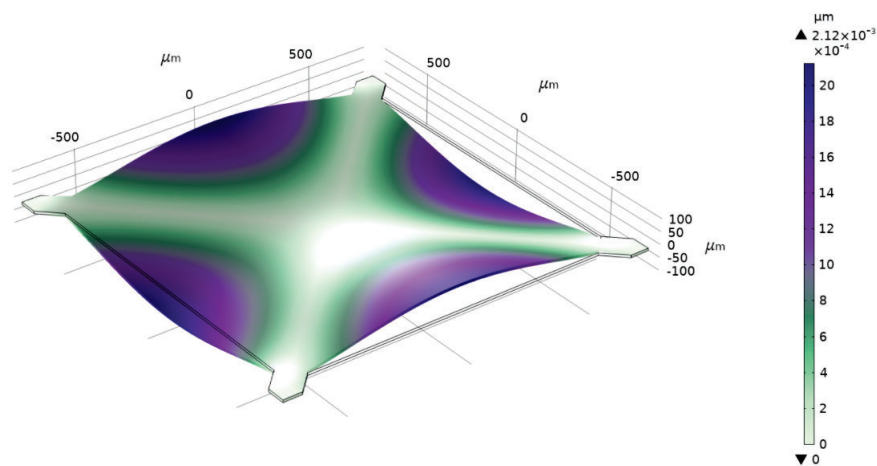
Figure 7.10: Eigenmode of a 1.5mm×1.5mm×10μm Trampoline (Unclamped) in Air at 58.154 kHz modeled using COMSOL®

Table 1: Predicted resonant frequencies of 2-D Drumhead (Clamped) Silicon PiezoMUMPs® membrane in air using Equation 4 and COMSOL® at the lowest mode.

Thickness (m)	Side length (m)	Resonant Frequencies 2-D Drumhead Using Equation 4 (Air) (kHz)	Resonant Frequencies 2-D Drumhead COMSOL (Air) Lowest Mode (kHz)
1.00E-05	2.00E-03	34.092	34.112
1.00E-05	1.00E-03	60.608	60.625
1.00E-05	5.00E-04	136.369	136.34
1.00E-05	5.00E-04	545.476	544.84

Table 2: Predicted resonant frequencies of 2-D Drumhead (Clamped) Silicon PiezoMUMPs® membrane in air using COMSOL® at the lowest and X mode.

Thickness (m)	Side length (m)	Resonant Frequencies 2-D Drumhead COMSOL (Air) Lowest Mode (kHz)	Resonant Frequencies 2-D Drumhead COMSOL (Air) X Mode (kHz)
1.00E-05	2.00E-03	34.112	1248
1.00E-05	1.00E-03	60.625	2217
1.00E-05	5.00E-04	136.34	4981
1.00E-05	5.00E-04	544.84	19852

Table 3: Predicted resonant frequencies of 2-D Trampoline (Unclamped) Silicon PiezoMUMPs® membrane in air using Equation 4 and COMSOL® at the lowest mode.

Thickness (m)	Side length (m)	Resonant Frequencies 2-D Trampoline Using Equation 4 (Air) (kHz)	Resonant Frequencies 2-D Trampoline COMSOL (Air) Low Mode (kHz)
1.00E-05	2.00E-03	12.778	10.503
1.00E-05	1.00E-03	22.717	19.157
1.00E-05	5.00E-04	51.114	43.12
1.00E-05	5.00E-04	204.458	173.11

Table 4: Predicted resonant frequencies of 2-D Trampoline (Unclamped) Silicon PiezoMUMPs® membrane in air using COMSOL® at the lowest and X mode.

Thickness (m)	Side length (m)	Resonant Frequencies 2-D Trampoline COMSOL (Air) Low Mode (kHz)	Resonant Frequencies 2-D Trampoline COMSOL (Air) X Mode (kHz)
1.00E-05	2.00E-03	10.503	32.905
1.00E-05	1.00E-03	19.157	58.154
1.00E-05	5.00E-04	43.12	130.15
1.00E-05	5.00E-04	173.11	514.84

Table 5: Predicted resonant frequencies of 2-D Drumhead (Clamped) PiezoMUMPs® membrane in water using water factor at the lowest mode.

Side length (m)	Water Factor	Resonant Frequencies 2-D Drumhead COMSOL (Water) Lowest Mode (kHz)
2.00E-03	0.2	68.22
1.00E-03	0.2	121.25
5.00E-04	0.2	272.68
5.00E-04	0.2	1089.68

Table 6: Predicted resonant frequencies of 2-D Drumhead (Clamped) PiezoMUMPs® membrane in water using water factor at the X mode.

Side length (m)	Water Mode	Resonant Frequencies 2-D Drumhead COMSOL (Water) X Mode (kHz)
2.00E-03	0.17	212.16
1.00E-03	0.17	376.87
5.00E-04	0.17	846.77
5.00E-04	0.17	3374.84

Table 7: Predicted resonant frequencies of 2-D Trampoline (Unclamped) PiezoMUMPs® membrane in water using water factor at the lowest mode.

Side length (m)	Water Factor	Resonant Frequencies 2-D Trampoline COMSOL (Water) Lowest Mode (kHz)
2.00E-03	0.67	7.04
1.00E-03	0.67	12.84
5.00E-04	0.67	28.89
5.00E-04	0.67	115.98

Table 8: Predicted resonant frequencies of 2-D Trampoline (Unclamped) PiezoMUMPs® membrane in water using water factor at the X mode.

Side length (m)	Water Mode	Resonant Frequencies 2-D Trampoline COMSOL (Water) X Mode (kHz)
2.00E-03	1.87	61.53
1.00E-03	1.87	108.75
5.00E-04	1.87	243.38
5.00E-04	1.87	962.75

7.2.6   Image Acquisition

For our microscale experiments, we used similar image acquisition techniques to those employed in the macroscale setup described in Section 7.1.2. A new microscope camera (Dino-Lite Edge AM73915MZTL 5.0MP Digital USB Microscope 10x 140x Metal USB 3.0 AMR) was used in order to accurately and precisely capture the microbeads (d = 50μm). The camera was connected via USB to a computer and mounted directly above the Chladni plate. The microscope took a specified number of frames per frequency outputted (0.0717 seconds per frame). With the addition of water, it took much longer for specific frequencies to create a Chladni figure. The frame number ranged from 50 to 1000 frames depending on the amplitude and frequency of the signal applied.

7.2.7   Image Processing and Object Identification

The macroparticle image acquisition techniques utilized on the macroscale were similar, but needed changes on the microscale due to differing particle sizes and the introduction of fluid. First, the images were geometrically transformed to correspond to a 2-D overhead view and cropped. The geometric transformation and cropping was first applied to a sample image and then applied uniformly to the remaining images in the data set.

The microbeads ($d = 50\mu$m) used in the microscale setup were red, starkly different from the dark silver of the solder beads used with the multimode membrane resonators. Instead of performing object identification via intensity thresholding in grayscale, the images were processed in full color to take advantage of the strong red color of the microbeads in object identification. The beads were analyzed by their color saturation content (Red, Blue, and Green). The red color saturation values had the largest variability and significance for identification as the microbeads themselves were red. Table 9 shows the specific design choices made in color thresholding. Too much or too little of one color would inadvertently filter out microbeads. After color thresholding, morphology operations were applied to the binary images to obtain better fidelity to bead dimensions. The images were first flood-filled with a "hole" of 25 pixels. By adjusting the "hole" size, it was possible to change the shape of the microbeads' outline. Subsequently, the same process described in Section 7.1.3 was applied to identify each particle as an object.

Table 9:   Threshold values used for red, green, and blue in the post-image processing.

Color Threshold Values (RGB)		
	Minimum	Maximum
Red	90	150
Green	0	15
Blue	0	15

7.2.8 Displacement Maps

Displacement maps for our microscale experiments were generated in a different manner than that used to generate displacement maps at the macroscale. Instead of averaging the displacement vectors from every 5th frame, the displacement vectors of frames 1 and 6, 2 and 7, 3 and 8, and so forth were averaged together. The inclusion of all frames increased post-image processing time. However, we were able to acquire a more comprehensive displacement map by using all frames acquired.

Subsequently, more improved displacement maps were created by using the weighted average based off the time elapsed between each frame. Five separate displacement maps were created using five separate frame intervals: 1, 2, 3, 4, and 5. For example, for a frame interval of 1, Frames 1 and 2, Frames 2 and 3, Frames 3 and 4, etc. were averaged until Frames 199 and 200. Similarly, for a frame interval of 2, frames 1 and 3, Frames 2 and 5, Frames 3 and 6, etc. were averaged until Frames 197 and 200. Subsequently, the five displacement maps were averaged based off the time elapsed between the frame intervals. For example, the time elapsed between Frame 1 and 2 was (ideally) one fifth of the time spent between Frames 1 and 6. Therefore, the displacement vectors calculated with frame intervals of 5 (e.g. Frame 1 and 6, Frame 2 and 7, etc.) should be 1/5 the weight of those calculated using a frame interval of 1 (i.g. Frame 1 and 2, Frame 2 and 3, etc.).

Further improvements were made by bypassing the intermediate frames entirely and only using the first and last frame. This was done by calculating any positive differences, that is the movement towards the gathering of particles in the first and last frame (i.e. Frames 1 and 200). This was done by using a Gaussian filter that was applied to the image to create a color gradient. A heat map depicting the clustering of particles was created and subsequently, the displacement map was created, but only including the positive difference vectors. This final improvement created the highest fidelity displacement maps that were able to bypass the circular particle movement that began to occur on the microscale. The generated displacement maps are shown in Section 9.2.4.

8 Experimental

8.1 Macroscale Manipulation - Chladni Plate in Air

A Chladni plate, 50mm×50mm×500μm^2 diced from a mechanical grade silicon wafer was mounted on a piezoelectric actuator (Piezomechanik/PSt 150/2x3/5) using adhesive (Super Glue). As in Zhou1, the polished side of the plate was oriented downwards to minimize reflections toward the camera. The computer was connected via USB to the signal generator (MokuLab®). The movement of the solder beads was captured using a microscope camera (Dino-Lite Edge AF4115ZTW 1.3MP Digital USB Microscope 2x 50x FLC), connected via USB to a computer and mounted directly above the Chladni plate. The schematic and experimental setup is shown in Figure 8.1.

A sinusoidal signal output of frequencies 1245Hz, 1976Hz, 3951Hz, 7902Hz, 11175Hz,

and 19912Hz was outputted in 6 different tests. These frequencies were selected based off of [30] and previous analytical computations described in-depth in Section 7.1.1. The frequencies outputted were programmed using MATLAB to have a 1Vpp or 2Vpp magnitude - dependent on the frequency used. Because the output of the signal generator was limited to a max voltage of 2Vpp, it was necessary to feed the signal through an amplifier (EPA104-203). The signal output was sent through the amplifier (gain ranging from 0-20x) and connected to the piezoelectric actuator, ultimately resulting in an output. We used output ranges between 5-25 Vpp. The DC offset was 0V. The output signal was then sufficient to drive the piezoelectric actuator and produce the Chladni figures produced [30] and shown in Figure 9.1.

The frequencies could be generated in sequential order or in non-sequential, randomized order allowing for versatility in the experiment. However, the solder beads were reapplied to fully cover the Chladni plate between each applied frequency in order to capture a sizable number of bead movements. Thus, the order in which each tested frequency was applied was not relevant as each test was separate and did not have an affect on the others.

Originally, sand particles ($d = 1$mm) were placed on top of the Chladni plate and formed Chladni figures in response to the resonant frequencies as pictured in Figure 9.1. However, the diameter of the sand particles averaged 1 mm (1000μm), much larger than needed. Thus, the sand particles were replaced with 750μm solder beads.
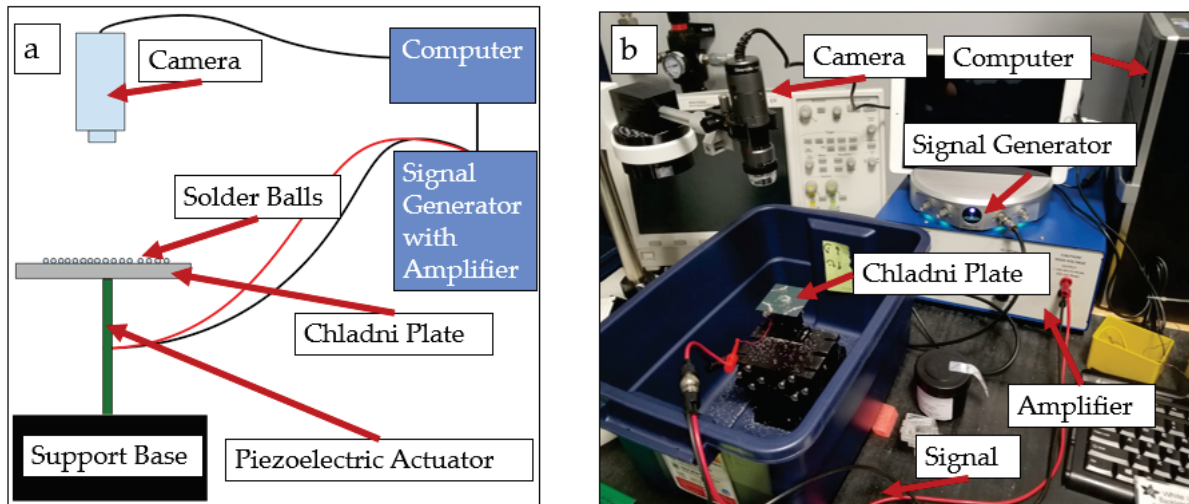

Figure 8.1: Macroscale manipulation with Chladni plate in air experimental setup. a) schematic b) photograph

8.2 Microscale Manipulation - Multimode Membrane Resonator in Water

The full die (8.5×8.5×0.001 mm) containing four quadrants (4.25×4.25×0.001 mm) of multimode membrane resonators was mounted on a piezoelectric actuator electric actuator (APC

841 6.25mm×6.25mm×.40mm) We used a standard non-conductive epoxy to connect the quadrant to the piezoelectric actuator. The piezoelectric actuator was connected to the ceramic package with conductive epoxy that doubled as a mechanical fastening and electrical connection. The computer was connected via USB to a signal generator (MokuLab®). Similar image acquisition techniques on the macroscale were used on the microscale.

The multimode membrane resonators were glued on top of the piezoelectric actuator, leaving an air bubble in between the resonators and the actuator. Like in [15], an air bubble was left to induce a standing wave pattern. This setup was placed in a chip package, allowing for more accessible and robust electrical connections to the piezoelectric actuator. The signal wire was soldered to the top electrode of the piezoelectric actuator, and the ground wire was soldered to the conductive bottom of the package which made electrical contact with the bottom electrode of the piezoelectric actuator through a conductive epoxy. Subsequently, an insulating varnish layer (Sprayon®Insulting Varnish) was sprayed onto the actuator and package in order to prevent shorts in the circuit with the addition of water. Microbeads (d = 50μm) were sonicated in de-ionized (DI) water to disperse the beads more uniformly in the liquid. Surfactant (Tween 80, 0.01% v/v) was added to minimize air bubble formation around the beads. Sonication was ineffective as a method of dispersing particles left for long periods as the particles settled to the bottom of the vial over a few hours. Merely shaking the vial by hand for 2 seconds was sufficient to disperse the particles throughout the solution.

A new microscope camera (Dino-Lite Edge AM73915MZTL 5.0MP Digital USB Microscope 10X 140X Metal USB 3.0 AMR) was used in order to accurately and precisely capture the microbeads (d = 50μm). The schematic and experimental setup is shown in Figure 8.2. More detailed photographs of the setup are shown in Figure 8.3. 50μL of the solution was deposited on top of the multimode membrane resonators using a micropipette.

The actuating signal was swept through a range of frequencies from 10 kHz to 1 MHz in steps of 10 kHz. Trials were conducted with both descending and ascending steps of frequency. This range of frequencies was determined as discussed in Section 7.2.5 and [15]. Each note was programmed using MATLAB to have a 1 Vpp magnitude and sinusoidal shape. The amplitude of the output was varied by changing the gain of the amplifier (EPA-104 230), ultimately resulting in output voltages between ranging between 5- 25 Vpp.
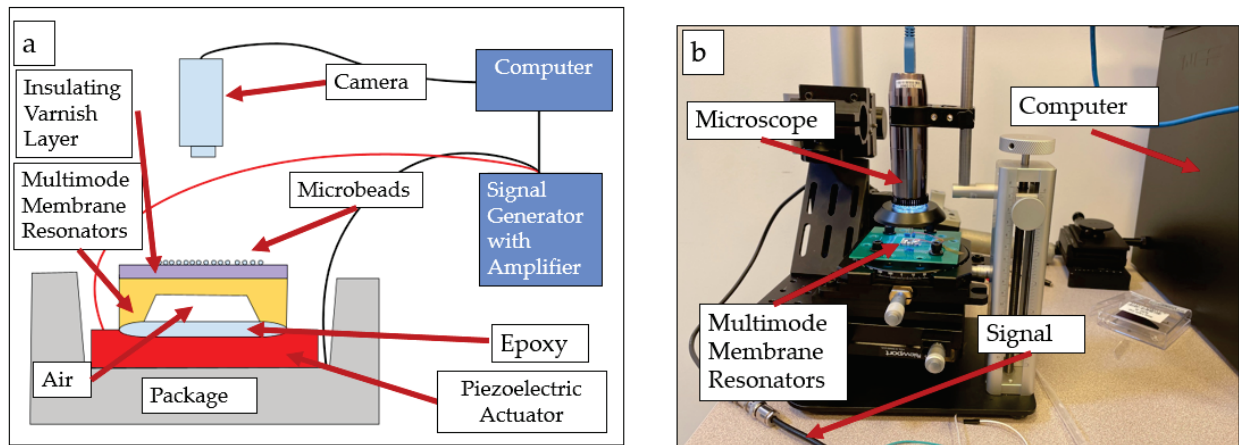
Figure 8.2: Microscale manipulation with multimode membrane resonators in water experimental setup. a) schematic b) photograph
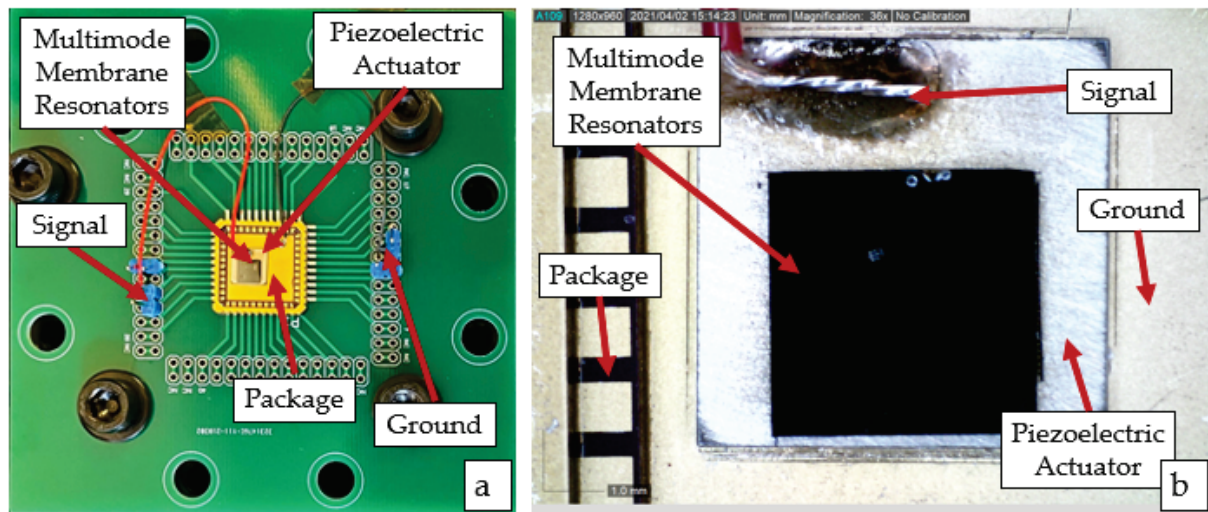

Figure 8.3: a) Photograph of microscale resonator platform. b) Close-up photograph of microscale resonator setup.

9   Results and Discussion

9.1   Macroscale Manipulation - Chladni Plate in Air

For the macroscale experiments, the image acquisition, image post-processing, and displacement map generation were successful and consistent with design predictions and [30]. The frequencies predicted in [30] matched with previous computations discussed in Section 7.1.1. Figure 9.1 shows one of the early trials conducted with sand particles taken after playing a note with a frequency of 3591 Hz. Later on, solder beads were used and formed Chladni figures in Figure 9.1.2.a.
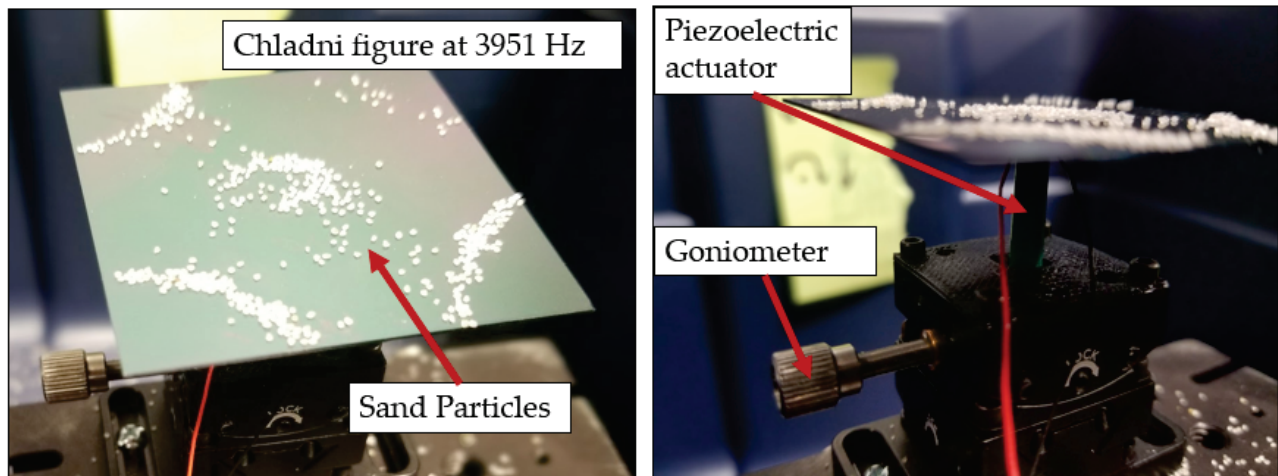
Figure 9.1: Picture of Chladni figure developed at 3951 Hz

9.1.1   Macroparticle Detection

The photos taken the 6-tested frequencies were processed through the post-image processing algorithm described in Section 7.1.3. The particles were object-identified as shown in Figure 9.2 at 3951 Hz.

9.1.2   Displacement Maps

Displacement maps were created for each resonant frequency through the process described in Section 7.1.4. A large displacement map for the movement of particles in response to a 7902 Hz note is seen in Figure 9.3. A figure with all test frequencies is shown in Figure 9.1.2.

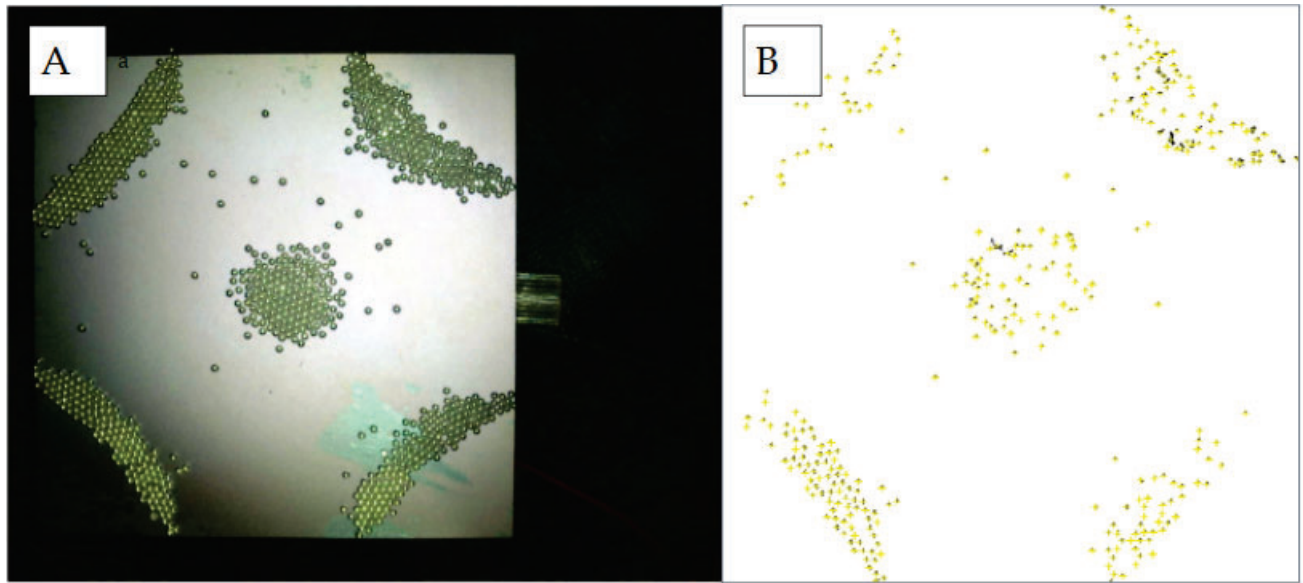Figure 9.2: a) Original picture of the Chladni plate pre-image processing b) Object identification on a cluster of solder beads. Yellow marks indicate identified particles.
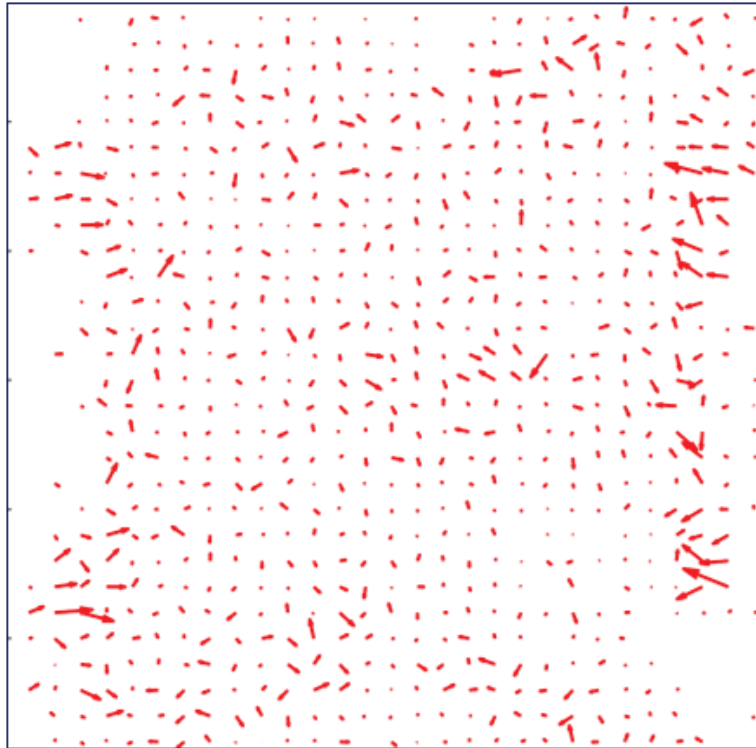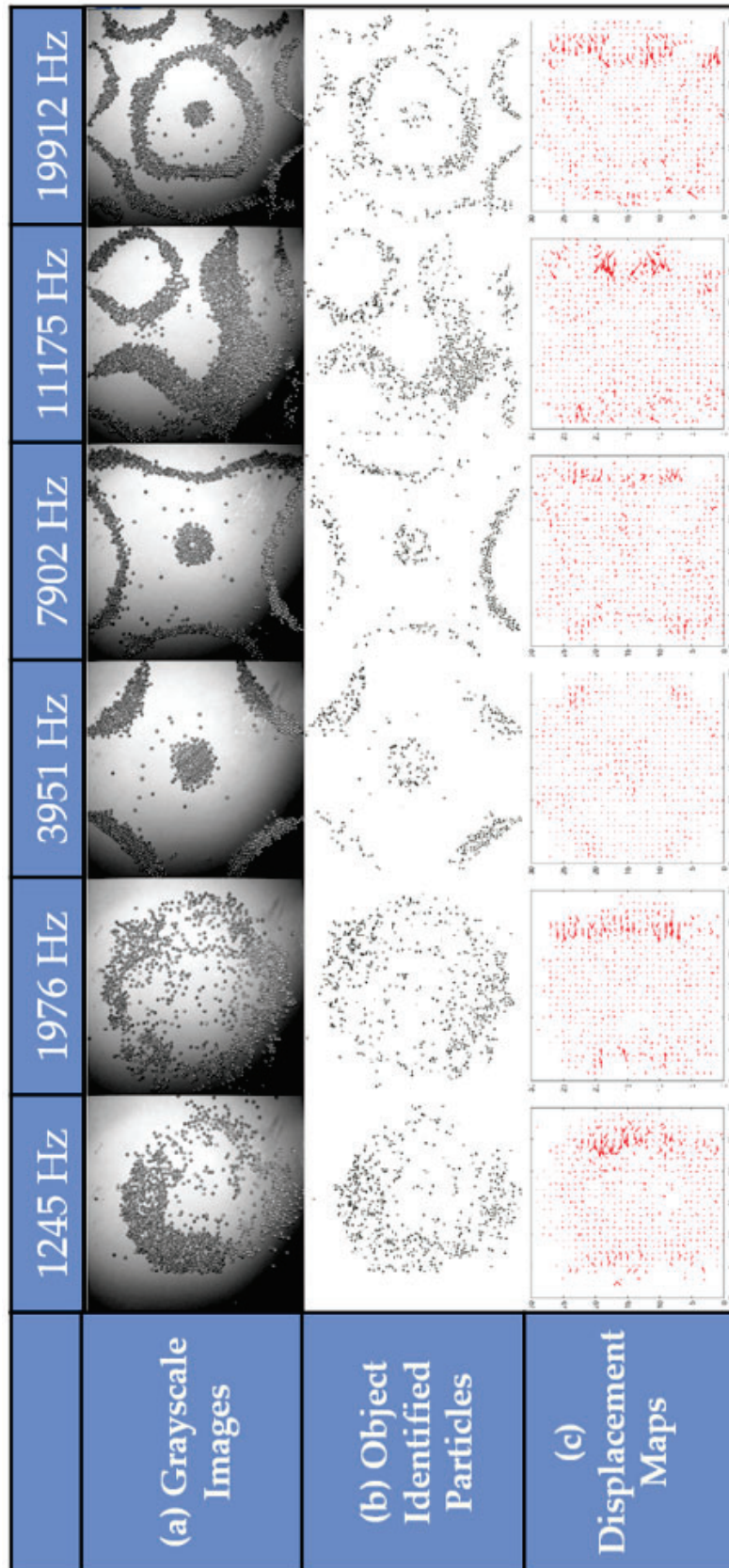

Figure 9.3: Displacement map at 7902 Hz

Figure 9.4: Photographs and processed images for Chladni plate experiments with various resonant frequencies.

9.1.3   Macroscale Experimental Issues

One issue we encountered on the macroscale was uneven resonance amongst the various tested frequencies. From Figure 9.1.2, it is clear that some frequencies were more resonant than others. For example, the figures formed in response to notes of 3.95kHz and 19.91kHz were strongly defined, which we identified with a strong response by the particles due to a strong amplitude of vibration of the Chladni plate. The vibrational amplitude of the oscillating Chladni plate was possibly larger with some frequencies and less with others. The beads moved more robustly in response to some frequencies compared to others.

Moving forward, there are a couple of ways to address this issue. One way is to increasing the duration of each note while maintaining a relatively low amplitude. This approach avoids loss of beads due to overdriving that can result by simply raising amplitude at all frequencies. It also circumvents the analytical and computational effort to dynamically adjust amplitude of driving voltages. On the other hand, the minimum amplitude must still be empirically determined and set so that all notes demonstrate some response. Another method is to dynamically change the voltage output of the signal generator based on the resonance of a particular frequency. However, this method requires more understanding of the specific resonances of a $50\text{mm}\times50\text{mm}\times500\mu\text{m}^2$ plate. However, it is also possible to empirically arrive at these values as well, similar to the process with creating displacement maps. Because the ultimate purpose of this experiment is to develop the control algorithm to be implemented on the microscale, a comprehensive study of the resonance of the macroscale Chladni plate was determined to not be a priority.

Another issue we encountered was the uneven tilt. Sensitivity of solder bead movement to the tilt of the Chladni plate was another issue encountered during experiments. While the goniometer placed under the Chladni plate was helpful in adjusting the tilt, it was extremely difficult to perfectly level the plate. For example, in Figure 9.1.2 at 11175 Hz, the Chladni figure was clearly assymmetric. One explanation is the uneven tilt resulting in the uneven gathering of particles, evident at the bottom half of the Chladni plate at 11175 Hz.

Another issue we encountered was uneven coupling. Looking at Figure 9.1.2.c, it is evident that some of the displacement maps are uneven, most notably those at 1245 Hz, 1976 Hz, and 11175 Hz. Because the piezoelectric actuator was glued to the plate manually, it is probable it was not exactly centered under the plate. Thus, the standing wave patterns induced in the Chladni plate were not entirely symmetrical, ultimately resulting in asymmetrical displacement maps.

Another issue we encountered was uneven lighting and glare. Initially, the image post-processing algorithm was unable to eliminate the glare from the uneven lighting in the room as depicted by Figure 9.5. Originally, we spent time and resources installing and using new lighting sources to increase the light in the dark spots - most notably in the corners. This method did not work as glare was further increased and dark spots left even darker. However, with an improved image post-processing algorithm, the glare and uneven lighting was eliminated.
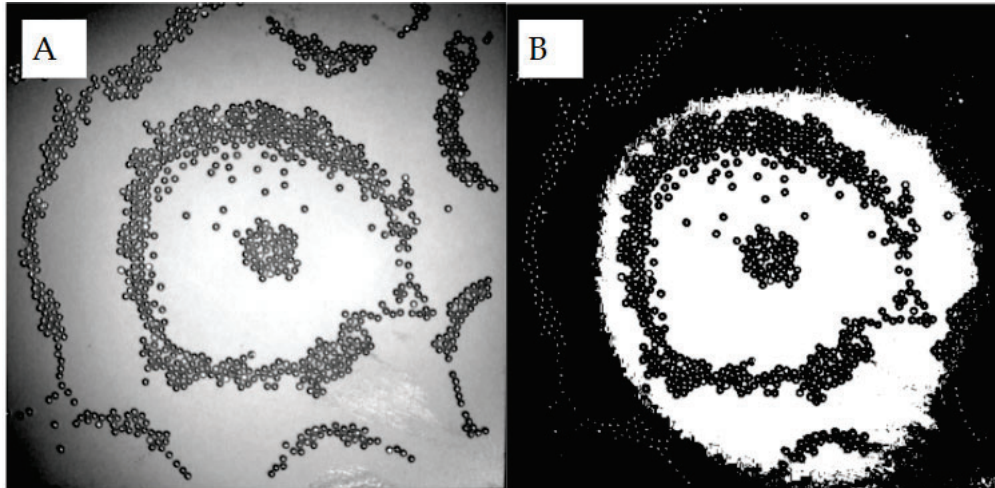
Figure 9.5: a) Chladni figure grayscale photo at frequency 19912 Hz with evident light glare b) Post-processed image with evident glare

9.1.4 Macroparticle Manipulation

As a proof of concept test, we manipulated the position of a single particle with a single note. The identified particle in Figure 9.6 was moved down the Chladni plate shown by the displacement map in Figure 9.7.

Figure 9.6: Object-identified single particle

By using the experimental data and developed image post-processing algorithms, it

Figure 9.7: Proof-of-concept displacement map demonstrating the correct and accurate ability to move particle using previously modeled resonances

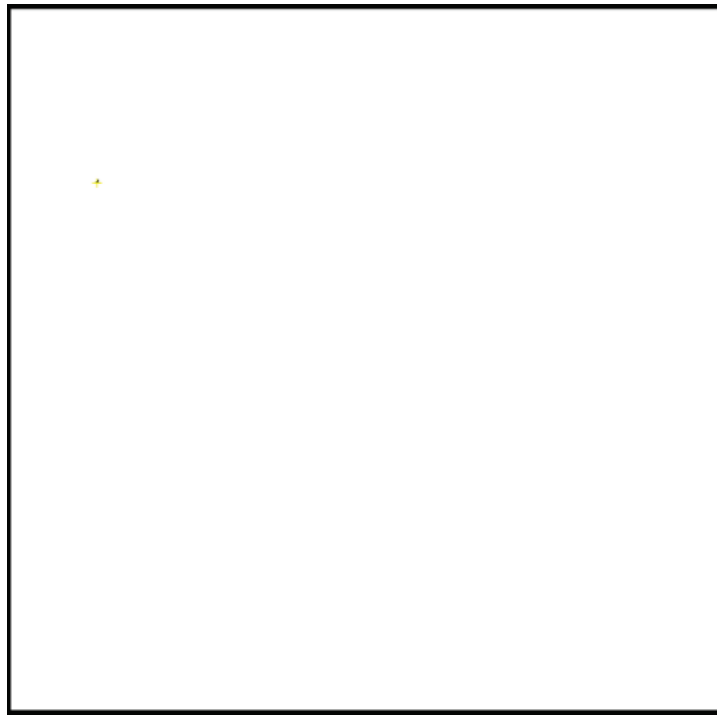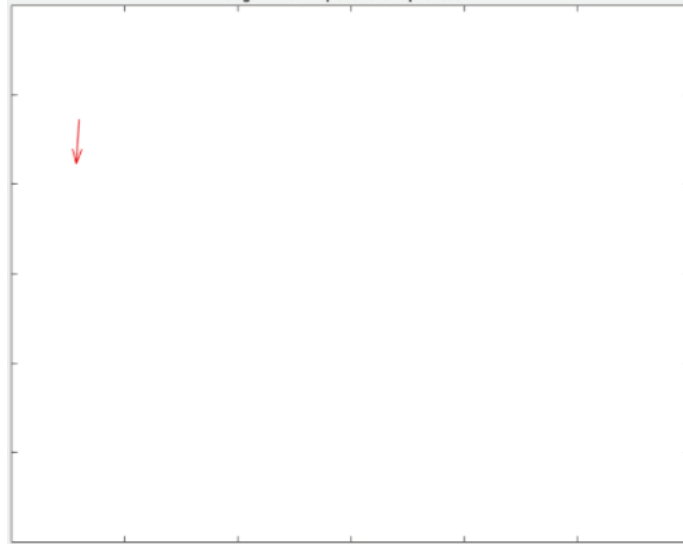should be possible in the future to manipulate a single particle on a Chladni plate. In theory, the intended coordinate or position would be an input into a MATLAB algorithm. Then, the path from the microrobot's current position to the intended position would be broken up into a set of waypoints. The microrobot's trajectory would track these waypoints in sequence. The algorithm would then loop through the saved displacement field maps and choose the note (frequency) that best fit the intended movement to arrive at the desired position. Then, the selected note would be played. This process would be repeated until the particle reaches its intended destination. One consideration is choosing waypoints that are close enough to one another. Choosing waypoints in close proximity would reduce the likelihood that the microrobot would stray from the intended path. Another consideration is particle size. For macroscale manipulation, the particle would be sub-mm.

9.2 Microscale Manipulation - 2-D Drumhead in Water

Following the macroscale experiments in air, we transitioned to testing microscale beads in water. We intended to use the image post-processing algorithms and particle imaging process. Though there were various membrane sizes and shapes, only the 2-D Drumhead (Clamped) in water was tested at time of writing. The image acquisition and object-identification algorithms were helpful, but needed refinement as described in Section 7.2.7. However the displacement map algorithm needed much bigger improvements (discussed later in Section 9.2.4.)

On the microscale, the beads conformed to patterns in response to the motion of the piezoelectric actuator under applied voltages of specific frequencies and amplitudes. The patterns formed were not as geometrically symmetrical as on the macroscale. One potential reason is the use of water that introduced numerous microfluidic phenomena including

acoustic streaming not seen on the macroscale. The typical Chladni figures that typically are seen were not as evident.

9.2.1 Classic Chladni or Inverse Chladni Figures

From Figure 9.9, it is clear that the beads are conforming to the center of the 2-D Drumhead (clamped) membrane. However, it is unclear however if the beads are forming inverse or classical Chladni figures as discussed in section 6.3.3. The answer lies in the modes of the various resonators. If the membranes are oscillating in the lowest mode, then Figure 9.9.a is clearly showing an inverse Chladni figure; however, it is unclear what mode the membrane was operating in. In a classical Chladni figure, the beads would form an "X" shape in the center of the membrane which may also explain the clustering of particles in Figure 9.9a. as well. Another reason is the locations where the beads are gathering most evidently are on the smallest resonators. The beads are relatively large compared to these resonators, so is difficult to observe the details of the figure. All we can see was that the beads gathered.

9.2.2 Resonant Frequency Analysis

The use of 1 kHz - 1 MHz in steps of 10 kHz predicted in the Section 7.2.5 provided a sufficient range of frequencies to observe resonance on the chip. The observed frequencies are clearly multiples of the predicted frequencies, indicative of eigenmodes. For example, the predicted 68 kHz is 1/4 of the observed 280 kHz, 1/9 of the 540 kHz, and 1/13 of 920 kHz. The predicted 272.7 kHz is 1/2 of the observed 540 kHz. The predicted 121 kHz is 1/4 of the observed 480 kHz and 1/5 of the observed 600 kHz. However, while we predicted only four of the lowest resonant frequencies, there were other resonant frequencies shown in Table 10 that were not necessarily multiples of the fundamental frequencies. One explanation is the analytical computations and COMSOL® simulation cannot account for the complicated interactions between the various parts: the coupling between the piezoelectric actuator and membrane resonators, position at which the signal activates the piezoelectric actuator, and the presence of mutual couplings between membrane resonators in proximity to each other. In addition, the multimode membrane resonators did not necessarily need to operate at their "natural frequency," but rather be driven by a large enough amplitude to induce movement in the microbeads despite not acting at a resonant frequency of the membrane [19]. Identifying the suitable resonant/non-resonant frequencies was achieved through observation - if the beads moved rapidly in response to a particular frequency, the frequency was denoted as "resonant" as seen in Table 10.

For the future, it would be helpful to extend the frequency range beyond 1 MHz as the predicted frequencies extend into the MHz range (>1MHz). Additionally, the step intervals should decrease from 10 kHz, as certain resonant frequencies may be skipped due to the large step intervals.

The same phenomena of uneven resonance was observed and is discussed in Section 9.1.3. Each frequency required different levels of amplitude to induce movement in the beads ranging from 5 Vpp - 25 Vpp.

Table 10:   Table that shows the predicted frequencies of the 2-D Drumhead (Clamped)
using COMSOL ouput values and a water damping factor.

Resonant Frequencies on the 2-D Drumhead (Clamped-Clamped) Low Mode	
Predicted (kHz)	Observed (kHz)
68.224	280
121.25	400
272.68	480
1089.68	540
	560
	600
	890
	920
	950

9.2.3   Image Post-Processing and Microparticle Detection

The image acquisition and image post-processing algorithms described in Section 7.2.6 were
successful as shown in Figure 9.8 at specifically 890 kHz. Even for smaller clusters of beads,
it was possible to properly detect the particles.

9.2.4   Displacement Maps

Accurate displacement maps at 890 kHz were developed as shown in Figure 9.11 and Figure
9.10. The initial displacement map algorithm developed on the macroscale was not entirely
helpful as shown in Figure 9.9 and needed refinement. The vectors were seemingly random
and did not conform to any clear pattern unlike on the macroscale.

One phenomena that the macroscale displacement map algorithm could not reconcile
was the "circular phenomena" observed most likely as a result of acoustic streaming. Unlike
in the macroscale air experiment, the beads exhibited a circular motion which was also
observed in [29]. In [29], it was suggested that this phenomena was related to the particles
moving from the position of one mode of resonance to another mode of resonance nearby in
frequency as explained previously in Section 6.2.3. Possibly if the frame rate is fast enough,
the circular motion creates a vector of small or zero magnitude. A displacement vector with
a magnitude of 0 is not useful. The initial, inaccurate displacement maps created at both
890 kHz and 440 kHz are shown Figure 9.9.

The use of only the initial and final frame was particularly useful and described previ-
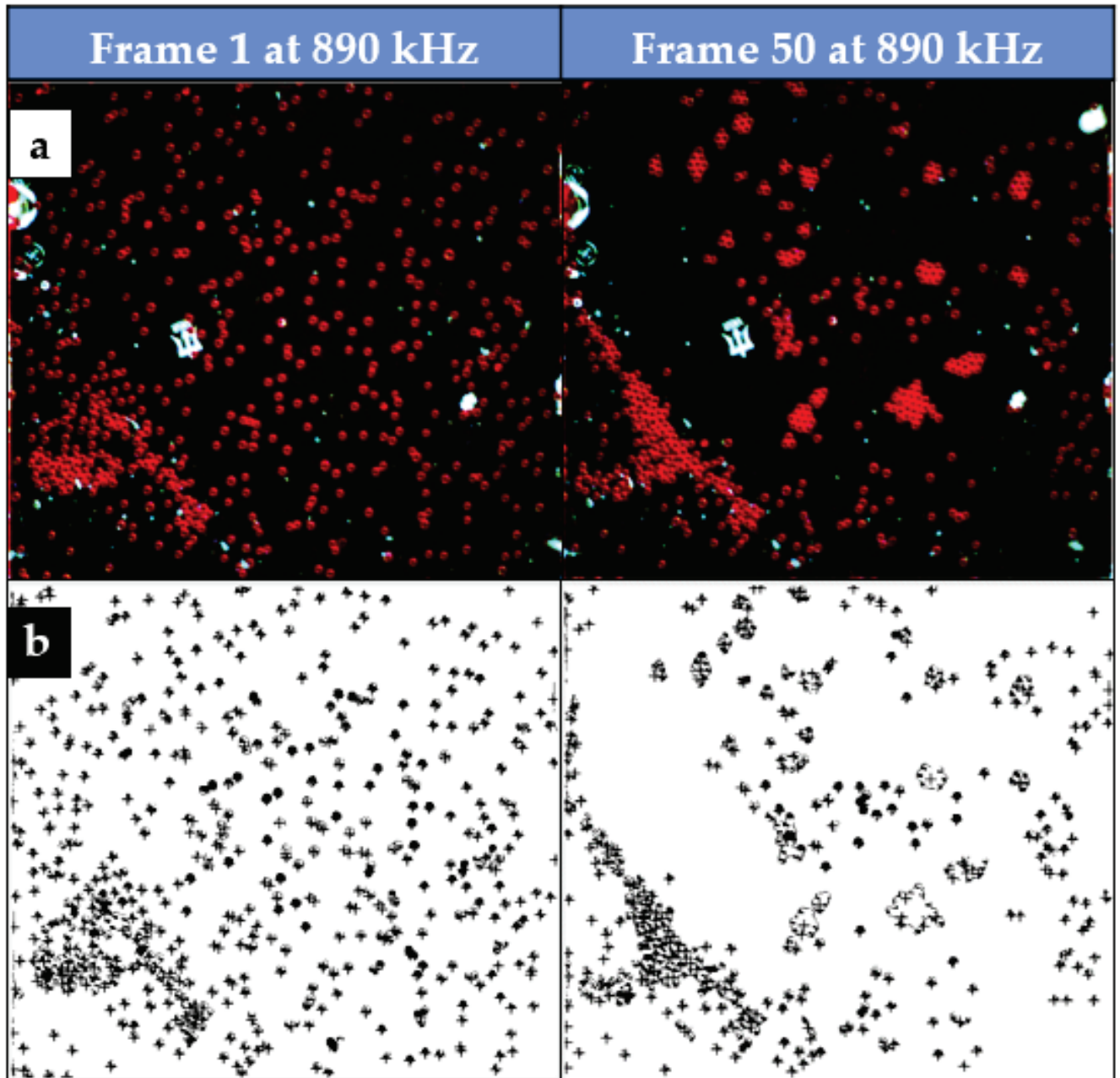ously in Section 9.2.4.

Figure 9.8: a) Microparticles (50μm) are imaged on the 2-D Drumhead (clamped) chip quadrant at 890 kHz b) Microparticles (50μm) identified effectively using image post-processing algorithms
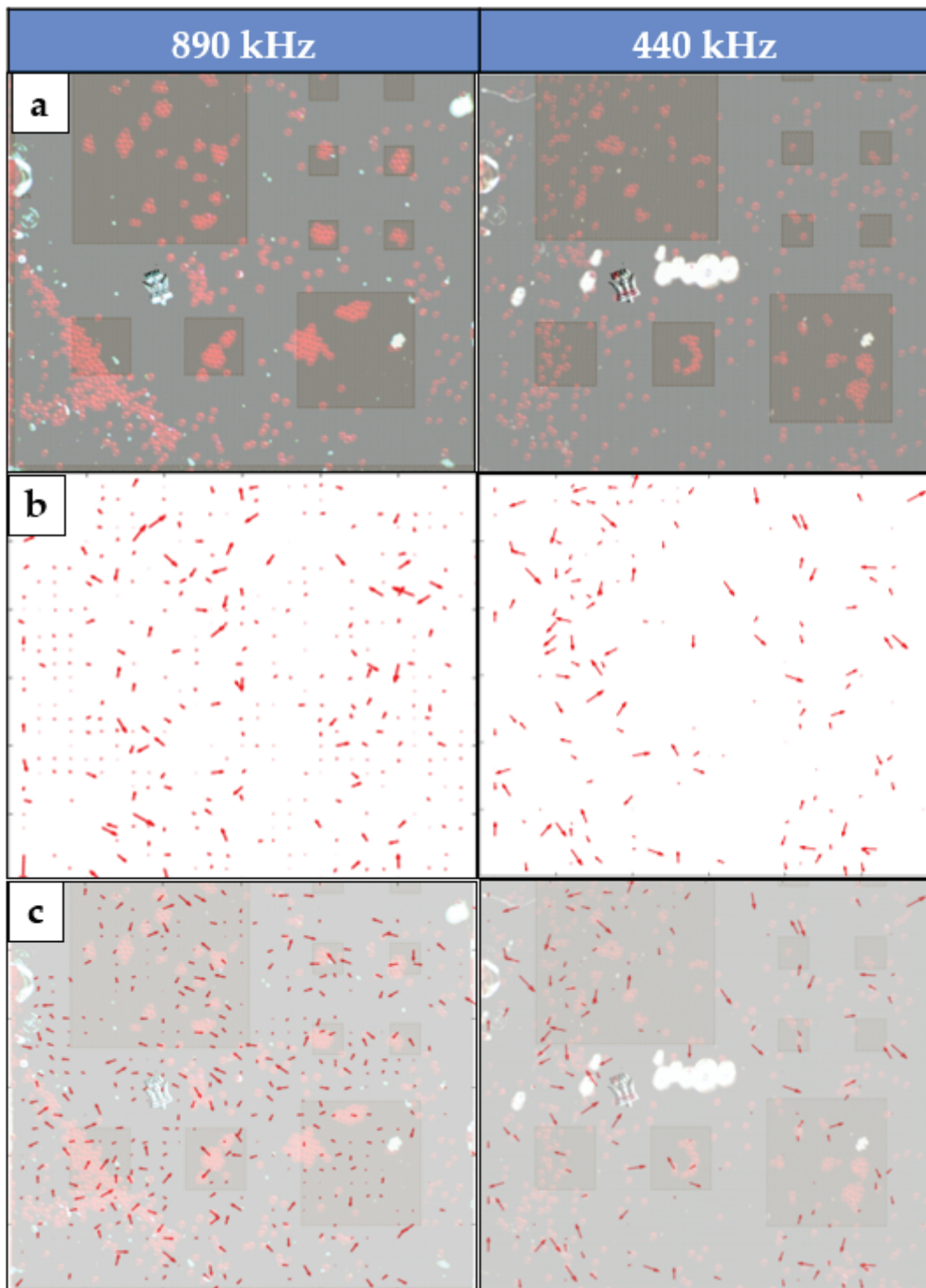
Figure 9.9: a) Microchip design was overlaid with the original images on the microscale at 890 kHz and 440 kHz b) Displacement maps were then made using algorithms from the microscale c) Displacement maps were overlaid with the original images on the microscale and microchip design
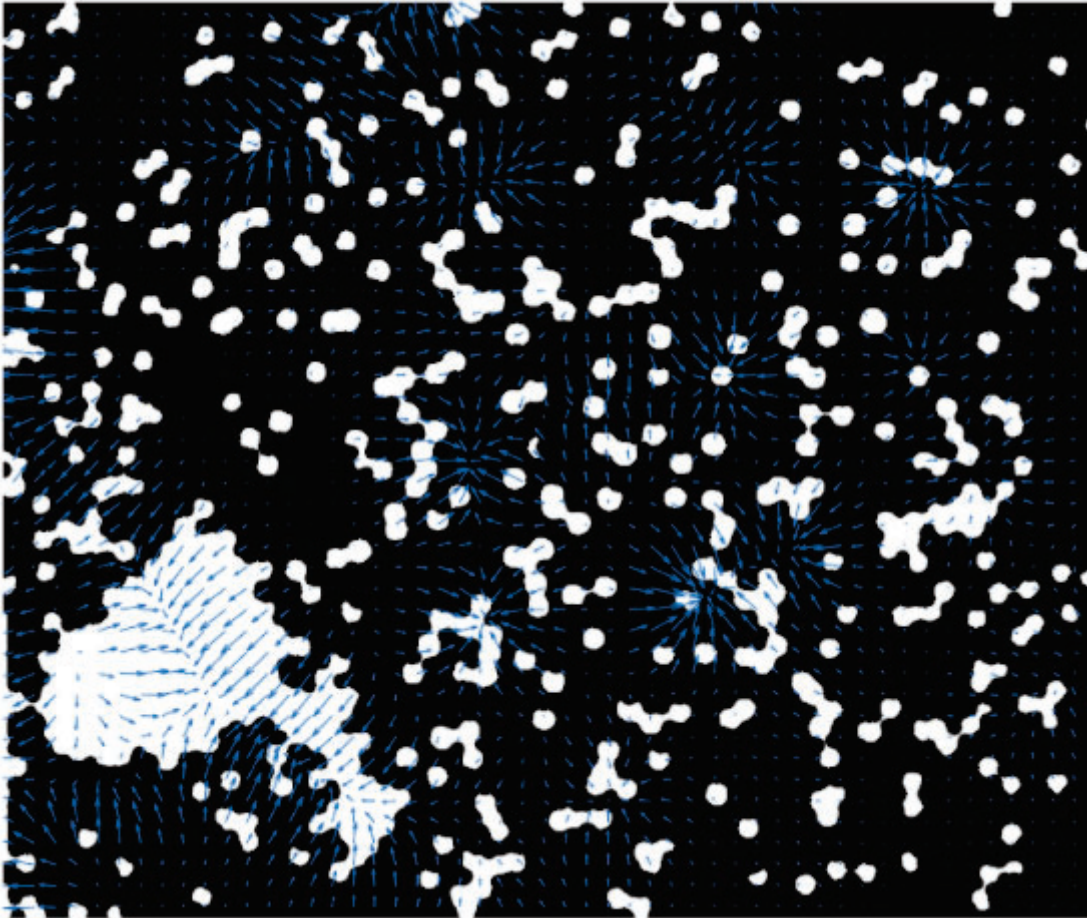
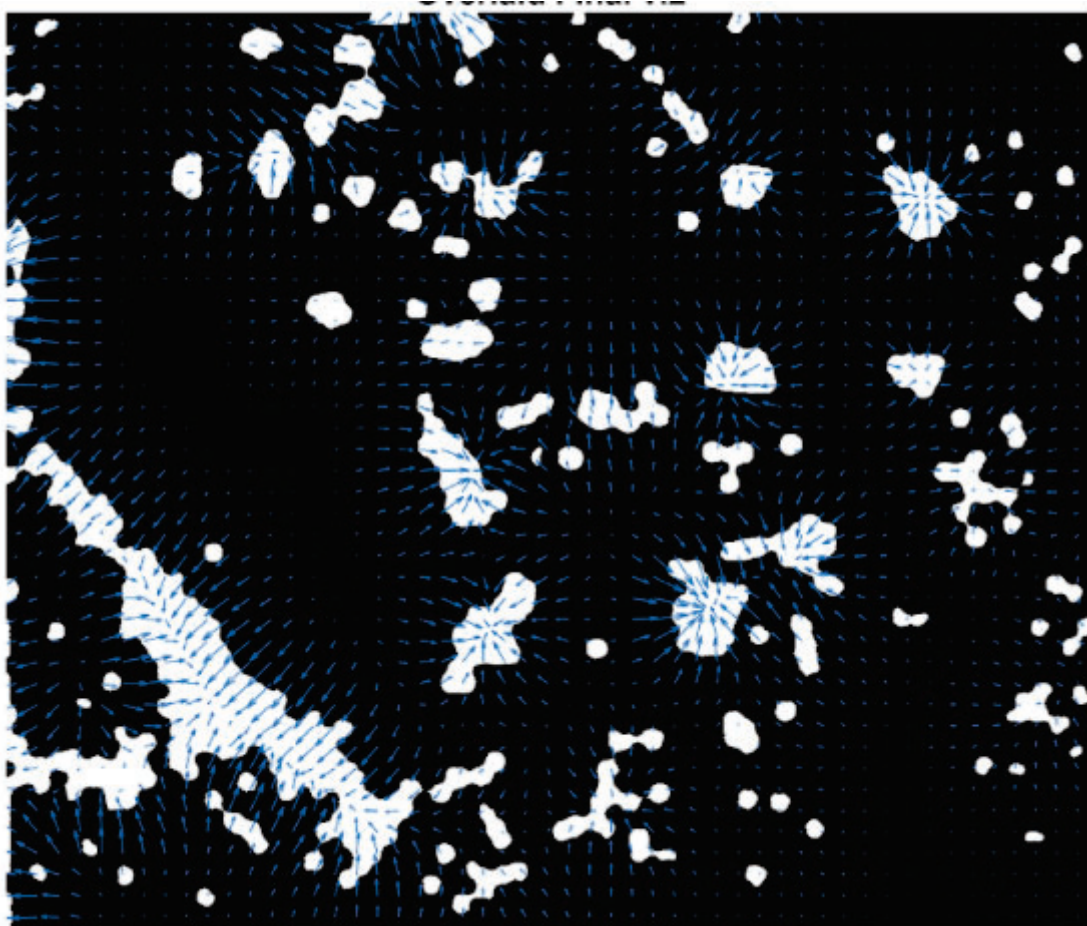Figure 9.10: Microscale displacement map at 890 kHz overlaid with the first frame

Figure 9.11: Microscale displacement map at 890 kHz overlaid with the final frame

9.3 Looking Forward

Moving forward, progress needs to be made on continuing to refine the displacement maps in fluid. As noted before, when using the same displacement map generation techniques employed at the macroscale on the microscale, we observed poor fidelity between the maps and the observed motion of particles. To address the issue, we revisited the image-pair spacing used to generate the maps as well as explore alternative displacement map generation methods based solely on final position of particles in response to a note. We will continue to find additional combinations of image-pairs and improve the current algorithms. Additionally, new sets of photos and data will be taken in order to refine the accuracy of the displacement maps.

Once new displacement maps are created more accurately, it will be possible to move on to the control part of the experiment, designing the computer algorithm to use the displacement maps to find the most effective frequencies to move the beads to their desired position on the microscale.

Once the control algorithm is refined, it is necessary to take images of the three other quadrants (2-D Trampoline, 1-D Beams, and Mixed Quadrant). If the previous displacement algorithm is successful, then it will be possible to model the movement on all quadrants with the same technique.

9.4 Conclusion

Overall, the objective of this project was to develop the experimental capability at USNA to perform two dimensional particle manipulation in water and in air through the use of macroscale and microscale Chladni plates and membranes. This goal was achieved using statistical analysis of particle movement on the Chladni plate/membrane to model displacement field maps. Manipulation and development of displacement maps was successful on the microscale. Additionally, a modified object-identification algorithm was successful on the microscale. The displacement map algorithm developed on the microscale was mostly successful, but needs improvement in order to account for microfluidic phenomena. Future work will be done to implement the displacement maps in controlling the microbeads. Ultimately, this research will help advance the current, incomplete understanding of the acoustics field in water at the microscale.

10   Glossary

- **Acoustic Radiation Force** - force on objects as a result of sound waves

- **Acoustic Streaming** - flow of liquid as a result of the absorption of an acoustic wave

- **Antinodes** - positions of maximum displacement of a standing wave in a resonant structure

- **Chladni Figures** - complex, symmetrical geometric patterns that particles on top of Chladni plates conform to in response to specific resonant frequencies

- **Chladni Plates** - plates supporting particles that conform to geometric patterns on the plate corresponding to the shapes of acoustic standing waves that are induced in the plate

- **COMSOL** ® - finite element method analysis program that allows the user to model various physics equations/phenomena

- **Displacement Map** - vector field that represents the motion of a bead/microrobot at any place on the Chladni plate in response to specific excitation

- **MEMSCAP** - a microfabrication firm offering multi-user microelectromechanical processes.

- **Microrobots** - robots with overall dimensions around 10 - 100 μm

- **Multi-Mode Membrane Resonator** - micrometer-scale thin membrane that oscillates similar to Chladni plates, but instead is supported and vibrated through anchors at its edges, rather than through an underlying, supporting post

- **Nodes** - positions of least displacement of a standing wave

- **Piezoactuator** - electrical device that converts an electrical signal into mechanical motion. Piezoelectric materials deform in response to the electric field imposed through the material, typically using voltages applied to electrodes on the faces of the piezoelectric material.

References

[1] Eigenfrequency analysis. https://www.comsol.com/multiphysics/eigenfrequency-analysis. Accessed: 2020-01-03.

[2] Lab on a chip. `https://www.flickr.com/photos/oistedu/40324601015/in/photostream/`. Accessed: 2020-12-05.

[3] Mems and nanotechnology exchange. `https://www.mems-exchange.org/MEMS/what-is.html`. Accessed: 2020-01-03.

[4] Micro-factory for miniaturization, portability and remote production. https://www.sbir.gov/sbirsearch/detail/234403. Accessed: 2020-01-12.

[5] Soimumps design handbook. `http://www.memscap.com/$__$data/assets/pdf$_$file/0019/1774/SOIMUMPs.dr.v8.0.pdf`. Accessed: 2020-01-03.

[6] Darpa shrimp challenge developing microrobots for disaster relief, 2018.

[7] Konstantin Glukh Allen Cowen, Greg Hames and Busbee Hardy. *PiezoMUMPs™ Design Handbook*. MEMSCAP Inc., 2015.

[8] Charles RP Courtney, Christine EM Demore, Hongxiao Wu, Alon Grinenko, Paul D Wilcox, Sandy Cochran, and Bruce W Drinkwater. Independent trapping and manipulation of microparticles using dexterous acoustic tweezers. *Applied Physics Letters*, 104(15):154103, 2014.

[9] Zachary R Gagnon. Cellular dielectrophoresis: applications to the characterization, manipulation, separation and patterning of cells. *Electrophoresis*, 32(18):2466–2487, 2011.

[10] David G Grier. A revolution in optical manipulation. *nature*, 424(6950):810, 2003.

[11] Feng Guo, Peng Li, Jarrod French, Zhangming Mao, Hong Zhao, Sixing Li, Nitesh Nama, James Fick, Stephen Benkovic, and Tony Huang. Controlling cell–cell interactions using surface acoustic waves. *Proceedings of the National Academy of Sciences*, 112:43–48, 11 2014.

[12] Feng Guo, Peng Li, Jarrod B French, Zhangming Mao, Hong Zhao, Sixing Li, Nitesh Nama, James R Fick, Stephen J Benkovic, and Tony Jun Huang. Controlling cell–cell interactions using surface acoustic waves. *Proceedings of the National Academy of Sciences*, 112(1):43–48, 2015.

[13] Stephen M. Heinrich and Isabelle Dufour. *Fundamental Theory of Resonant MEMS Devices*. Wiley, 2015.

[14] COMSOL Inc. How Do Chladni Plates Make It Possible to Visualize Sound?, year = 2018, url = https://www.comsol.com/blogs/how-do-chladni-plates-make-it-possible-to-visualize-sound/, urldate = 2019-12-28.

[15] H. Jia, X. Liu, and P. X. . Feng. Manipulating and patterning micro/nanoparticles in liquid using multimode membrane resonators. In *2018 IEEE Biomedical Circuits and Systems Conference (BioCAS)*, pages 1–4, Oct 2018.

[16] Hao Jia, Hao Tang, and Philip X.-L. Feng. Standard and inverse microscale chladni figures in liquid for dynamic patterning of microparticles on chip. *Journal of Applied Physics*, 124(16):164901, 2018.

[17] Lawrence E. Kinsler, Austin R. Frey, Alan B. Coppens, and James V. Sanders. *Fundamentals of Acoustics*. 1950.

[18] JO Kwon, JS Yang, SJ Lee, K Rhee, and SK Chung. Electromagnetically actuated micromanipulator using an acoustically oscillating bubble. *Journal of Micromechanics and Microengineering*, 21(11):115023, 2011.

[19] Kourosh Latifi, Harri Wijaya, and Quan Zhou. Motion of heavy particles on a submerged chladni plate. *Phys. Rev. Lett.*, 122:184301, May 2019.

[20] Junjun Lei. Formation of inverse chladni patterns in liquids at microscale: roles of acoustic radiation and streaming-induced drag forces. *Microfluidics and Nanofluidics*, 21, 03 2017.

[21] Ruei-Zeng Lin, Chen-Ta Ho, Cheng-Hsien Liu, and Hwan-You Chang. Dielectrophoresis based-cell patterning for tissue engineering. *Biotechnology Journal: Healthcare Nutrition Technology*, 1(9):949–957, 2006.

[22] G. Lucarini, S. Palagi, A. Levi, B. Mazzolai, P. Dario, A. Menciassi, and L. Beccai. Navigation of magnetic microrobots with different user interaction levels. *IEEE Transactions on Automation Science and Engineering*, 11(3):818–827, July 2014.

[23] Vivien Marx. Biophysics: Using sound to move cells. *Nature methods*, 12:41–4, 12 2014.

[24] Jenelle Piepmeier, Samara Firebaugh, and Caitlin Olsen. Uncalibrated visual servo control of magnetically actuated microrobots in a fluid environment. *Micromachines*, 5(4):797–813, 2014.

[25] P. H. Tuan, J. C. Tung, H. C. Liang, P. Y. Chiang, K. F. Huang, and Y. F. Chen. Resolving the formation of modern chladni figures. *EPL (Europhysics Letters)*, 111(6):64004, sep 2015.

[26] P. H. Tuan, C. P. Wen, P. Y. Chiang, Y. T. Yu, H. C. Liang, K. F. Huang, and Y. F. Chen. Exploring the resonant vibration of thin plates: Reconstruction of chladni patterns and determination of resonant wave numbers. *The Journal of the Acoustical Society of America*, 137(4):2113–2123, 2015.

[27] Henk van Gerner, Ko Weele, Martin Hoef, and Devaraj Meer. Air-induced inverse chladni patterns. *Journal of Fluid Mechanics*, 689:203 – 220, 12 2011.

[28] Henk Jan van Gerner, Martin A. van der Hoef, Devaraj van der Meer, and Ko van der Weele. Inversion of chladni patterns by tuning the vibrational acceleration. *Phys. Rev. E*, 82:012301, Jul 2010.

[29] Gaël Vuillermet, Pierre-Yves Gires, Fabrice Casset, and Cédric Poulain. Chladni patterns in a liquid at microscale. *Phys. Rev. Lett.*, 116:184501, May 2016.

[30] Quan Zhou, Veikko Sariola, Kourosh Latifi, and Ville Liimatainen. Controlling the motion of multiple objects on a chladni plate. *Nature communications*, 7:12764, 09 2016.

[31] Xiaozhu Zhou, Freddy Boey, Fengwei Huo, Ling Huang, and Hua Zhang. Chemically functionalized surface patterning. *Small*, 7(16):2273–2289, 2011.